

**APPENDIX IV**  
**DETAILS OF CASK RESPONSE TO FIRE ACCIDENTS**

## TABLE OF CONTENTS

IV.1.	Introduction .....	7
IV.2.	CAFE Finite Volume Domain and Boundary Conditions .....	8
IV.3.	The Rail-Steel Cask.....	11
IV.3.1	Geometric Consideration .....	11
IV.3.2	Rail-Steel Cask Thermal Behavior and Model Assumptions.....	19
IV.3.3	Rail-Steel Cask Materials and Thermal Properties.....	21
IV.3.4	Rail-Steel Cask, Finite Element Model and Boundary Conditions .....	29
IV.3.5	Rail-Steel Cask Thermal Analysis Results .....	31
IV.4.	Rail Cask with Lead Shielding.....	42
IV.4.1	Geometry Considerations .....	42
IV.4.2	Rail-Lead Cask Thermal Behavior and Model Assumptions.....	45
IV.4.3	Rail-Lead Cask Materials and Thermal Properties.....	48
IV.4.4	Rail-Lead Cask Finite Element Model .....	53
IV.4.5.	Rail-Lead Cask Thermal Analysis Results .....	54
IV.5	Truck Cask with Depleted Uranium .....	65
IV.5.1	Geometric Considerations .....	65
IV.5.2.	Truck-DU Thermal Behavior and Model Assumptions.....	67
IV.5.3	Truck-DU Materials and Thermal Properties .....	68
IV.5.4	Truck-DU P-Thermal Finite Element Model .....	71
IV.5.5	Truck-DU Cask Thermal Analysis Results .....	72
IV.6	CAFE Benchmark.....	74
IV.6.1	Large Calorimeter Test and Benchmark Results.....	75
IV.6.2	Small Calorimeter Test and Benchmark Results.....	77
IV.6.3	Summary of Benchmark Results .....	78
IV.7	Summary.....	78

## LIST OF FIGURES

Figure IV-1. CAFE three-dimensional domain: (a) CAFE regulatory fire, (b) cask on ground and at the center of the pool, (c) cask on the ground and 3 m (10 ft) from the edge of the pool, (d) cask on the ground and 18.3 m (60 ft) from the edge of the pool.....	10
Figure IV-2. Rail-Steel cask transportation system. ....	11
Figure IV-3. Rail-Steel cask: (a) assembly of MPC and overpack, and (b) cask with limiters (Holtec 2004). ....	12
Figure IV-4. Rail-Steel cask overpack: (a) cross-sectional view through the center of the cask, (b) cross-sectional view through the mid-plane of the overpack (Holtec 2004). ....	13
Figure IV-5. Rail-Steel cask MPC: (a) cross-sectional view through the axis of the cask, (b) cross-sectional through the midplane of the overpack (Holtec, 2004). ....	14
Figure IV-6. Fuel assembly (Holtec, 2004) (a) and fuel rod (b). ....	16
Figure IV-7. Fuel-basket region (left) and equivalent fuel-basket region (right). (Holtec, 2004). ....	17
Figure IV-8. Rail-Steel cask upper (a) and lower (b) impact limiters (Holtec, 2004). ....	18
Figure IV-9. Rail-Steel cask finite element mesh. ....	30
Figure IV-10. Rail-Steel Cask Regulatory Uniform Heating Results (P-Thermal).....	32
Figure IV-11. Rail-Steel cask CAFE regulatory fire. ....	34
Figure IV-12. Rail-Steel cask CAFE fire with cask on ground and at the pool center.....	36
Figure IV-13. Rail-Steel cask CAFE fire with cask on ground 3.0 m (10 ft) from the edge of the pool.....	38
Figure IV-14. Rail-Steel cask CAFE fire with cask on ground 18.3 m (60 ft) from the edge of the pool.....	40
Figure IV-15. Rail-Lead cask components with the direct loaded fuel basket shown to the right (NAC International, 2004). ....	43
Figure IV-16. Cross-section view of the Rail-Lead cask with the directly loaded fuel basket. ....	44
Figure IV-17. Axial burn up profile for the directly loaded fuel basket (NAC International, 2004). ....	46
Figure IV-18. Three-dimension, quarter section of the directly loaded basket. The helium material is not shown. ....	47
<b>Figure IV-19. The Rail-Lead cask mesh. ....</b>	<b>53</b>
Figure IV-20. Rail-Lead cask regulatory uniform heating results. ....	55
Figure IV-21. Rail-Lead cask CAFE regulatory fire. ....	57
Figure IV-22. Rail-Lead cask on ground at the pool center. ....	59
Figure IV-23. Rail-Lead cask on ground 3.0 m (10 ft) from the edge of the pool. ....	61
Figure IV-24. Rail-Lead cask on ground 18.3 m (60 ft) from the edge of the pool. ....	63
Figure IV-25. Components of Truck-DU cask (General Atomics 1993). ....	65
Figure IV-26. Truck-DU cask mesh. ....	71
Figure IV-27. CAFE three-dimensional domain with Truck-DU cask on ground. ....	72
Figure IV-28. Truck-DU cask on ground at the pool center. ....	73
Figure IV-29. Large calorimeter fire test: (a) test setup and (b) fire fully engulfing the calorimeter. ....	75

Figure IV-30. Side view (looking from the north) of calorimeter and test setup. Note: the calorimeter is centered with the pool. This drawing is not to scale.....	76
Figure IV-31. CAFE benchmark results using fully engulfed large calorimeter: (a) temperatures average along the 0, 90, 180, and 270 degree side looking at the calorimeter from the negative z-direction, and (b) temperatures averaged over each ring starting from Ring 1 located on the positive side of the z-axis. ....	76
Figure IV-32. CAFE benchmark results using a small calorimeter 1.5m (4.9ft) from the edge of the fire.....	78

### LIST OF TABLES

Table IV-1. Axial burn up profile in the active fuel region of the Rail-Steel cask.....	19
Table IV-2. Thermal conductivities for the Rail-Steel cask materials.....	22
Table IV-3. Specific heat for the Rail-Steel cask materials.....	23
Table IV-4. Densities for the Rail-Steel cask materials.....	24
Table IV-5. Emissivity for some of the Rail-Steel cask materials and paints.....	24
Table IV-6. Effective thermal conductivity for the fuel-basket region.....	26
Table IV-7. Effective thermal conductivity of the aluminum heat conduction elements.....	27
Table IV-8. Effective thermal conductivity of the intermediate shells in the in-plane directions.....	28
Table IV-9. Effective conductivity of the neutron shield region.....	28
Table IV-10. Thermal conductivities for the Rail-Lead cask materials.....	49
Table IV-11. Specific heat for the Rail-Lead cask materials.....	49
Table IV-12. Densities for the Rail-Lead cask materials.....	50
Table IV-13. Emissivity for some of the Rail-Lead cask materials.....	50
Table IV-14. Effective thermal properties of the directly loaded fuel basket.....	52
Table IV-15. Effective thermal conductivities for the neutron shield region of the Rail-Lead cask.....	53
Table IV-16. Axial burn up profile in the active fuel region of the Truck-DU cask.....	67
Table IV-17. Thermal conductivities for the Truck-DU cask materials.....	69
Table IV-18. Volumetric Specific heat for the Truck-DU cask materials.....	69
Table IV-19. Effective thermal conductivities for the Truck-DU cask materials.....	70
Table IV-20. Effective volumetric specific heat for the Truck-DU cask materials.....	70



## APPENDIX IV

### DETAILS OF CASK RESPONSE TO FIRE ACCIDENTS

#### IV.1. Introduction

Thermal analyses of Rail-Steel, Rail-Lead, and Truck-DU cask types were performed to obtain the thermal response of these casks to the fire accident scenarios described in Chapter 4. The approach used to model these casks is similar to the ones used in the HI-STAR 100 and NAC-STC Safety Analysis Reports (SARs) (Holtec International, 2004, NAC International, 2004) and in the GA-4 Final Design Report (FDR) (General Atomics, 1993), a combination of one-dimensional thermal resistance analysis (Incropera and Dewitt, 1996), and two- and three-dimensional finite element modeling. Thermal resistances are used to obtain effective thermal properties for several geometrically complex regions of the casks. These homogenized regions are then added back to the finite element model with the equivalent effective properties. This process eliminated some of the finite element discretization complexities inherent in the models, while at the same time keeping the essential thermal response of the casks.

Deleted: A t

Deleted: i

Deleted: is

For the Rail-Steel and Truck-DU casks, thermal resistance analysis reported in the Rail-Steel cask SAR (Holtec International, 2004) and in the Truck-DU cask FDR (General Atomic, 1993), respectively, are used, but modified where necessary to reflect the current study as will be touched on later in sections of this Appendix. The approach used to model the Rail-Lead cask is similar to the approach used in the Rail-Lead cask SAR (NAC International, 2004). The only exception is in how the contents of the cask are modeled. In the Rail-Lead cask SAR, the fuel-basket region and the rest of the overpack are modeled explicitly using a three-dimensional, quarter-section of the cask to obtain a steady-state solution. The maximum temperature difference between the center of the fuel-basket region and the inner wall of the overpack obtained in the steady-state solution is then used to calculate the fuel-basket cladding temperature for the regulatory uniform heating flux (see 10 CFR 71.73), which did not include a fuel-basket region.

In this study, a three-dimensional, quarter section of the fuel basket is used to obtain effective thermal properties for the Rail-Lead cask, fuel basket. The fuel-basket region is replaced in the full-scale, three-dimensional, finite element model using effective properties for the homogenized basket region. With the exception of the fuel basket region, results in the Rail-Lead cask SAR are used to obtain the thermal response of this cask, with minor changes to reflect the current study. Results taken from the Rail-Steel and Rail-Lead cask SARs and from the Truck-DU cask FDR are checked where possible using formulas taken directly from these reports or using formulas derived from independent analysis.

Some boundary conditions and material properties are slightly different from those used in the Rail-Steel and Rail-Lead cask SARs, and in the Truck-DU cask FDR. The intent of this thermal analysis is to determine the temperature of critical components during and after a hypothetical fire accident, using material properties and boundary conditions that closely resemble the conditions in a real fire accident. Since realistic boundary conditions are sometimes difficult to implement using available data and/or current analysis tools, some simplifications had to be

**Comment [csb1]:** I would use "actual boundary conditions related to a severe fire" instead, since the impression of this statement is that applying realistic boundary conditions is difficult to do...this may confuse someone and lead them to thinking that the boundary conditions you did apply are not realistic...even if they are conservative.

made. For example, the insulation material used in the neutron shields of both casks is assumed to decompose completely when its operational temperature limit is reached. In such cases, conservative assumptions are made to maximize heat input to the casks, as is done in both SARs cited above. In the case of material properties, those presented in the SARs are preferred, followed by those in standard thermal textbooks and journals. For some materials, properties are available, but only over a limited temperature range. In such cases, the value available at the highest temperature is used for higher temperatures.

As mentioned in Chapter 4, MSC PATRAN-Thermal (P-Thermal) (MSC, 2008) is the finite element heat transfer code used to solve the internal thermal response of the Rail-Steel and Rail-Lead casks in the regulatory uniform heating scenario. This scenario effectively simulates fire conditions using a spatially uniform radiation flux over the external surfaces of the casks as established in 10 CFR 71.73. CAFE (Container Analysis Fire Environment) is the computational fluid dynamics (CFD) code used to generate the fire environment for the CAFE regulatory and CAFE non-regulatory scenarios described in Chapter 4. For these scenarios, CAFE and P-Thermal are coupled together to obtain the thermal response of the Rail-Steel and Rail-Lead casks. CAFE generates more realistic fire conditions on the external surfaces of the casks, as opposed to spatially uniform heating conditions. P-Thermal uses CAFE-predicted, external conditions to calculate the internal thermal response of the casks.

Three fire accident scenarios different from the HAC regulatory fire configuration are analyzed for the rail casks, while one fire accident scenario, the most severe configuration of the rail cask analysis, is analyzed for the truck cask except with a fire lasting one hour, as described in Chapter 4. These scenarios represent the accident case in which the fuel pool and the cask are concentric with each other (fully engulfing), or separated by one rail car width, or one rail car length.

In the following sections, the geometry, material properties, and boundary conditions used to model the Rail-Steel, Rail-Lead, and Truck-DU casks are described, and results that supplement discussions in Chapter 4 are shown. The three-dimensional domain and the boundary conditions used in the CAFE runs are described first, followed by the geometry and boundary conditions used in the Rail-Steel and Rail-Lead cask analyses utilizing the P-thermal finite element models. Finally, the results from two CAFE runs used to benchmark the code are presented and discussed to demonstrate the validity of the CAFE code for these types of analyses.

## **IV.2. CAFE Finite Volume Domain and Boundary Conditions**

CAFE (Suo-Antilla et al., 2005) uses the finite volume approach with orthogonal Cartesian discretization to solve: (1) the three momentum equations for predicting the velocity and momentum field, (2) the mass continuity equation, (3) the energy equation for predicting the temperature field, (4) the equation of state, (5) a number of scalar transport equations for tracking the flow of species, and (2) two transport equations to solve thermal radiation within and external to the fire. CAFE uses a variable density algorithm (Pressure-Implicit Split-Operator, or PISO) to obtain a velocity field which satisfies both the momentum and continuity equations. CAFE has a number of turbulence models, but for this study a large eddy simulation formulation is used. Thermal radiation transport within and near the fires is split into two types:

diffusive radiation inside the flame zone and clear air radiation outside the flame zone. Diffusive thermal radiation transport is modeled with the Rosseland approximation. Clear air radiation outside the flame zone is modeled using view factor methods.

CAFE is coupled to P-Thermal through a set of user-supplied subroutines that pass temperature and thermal heat flux data between both codes. CAFE uses a specialized scheme to map the temperature and heat fluxes to the exterior surfaces of the finite element model (Suo-Antilla et al., 2005). MSC PATRAN is the front-end code employed to generate the material database, the finite element discretization, and the boundary conditions used by P-Thermal. It is through a special boundary condition, setup in PATRAN, that CAFE and P-Thermal are able to exchange data.

Figure IV-1 illustrates the domain configurations used in the CAFE fire scenarios discussed in Chapter 4. Figure IV-1(a) shows the computational fluid dynamics domain used for the CAFE regulatory run, and Figure IV-1(b) through Figure IV-1(d) show the domain for the CAFE non-regulatory runs. As explained in Chapter 4, all non-regulatory CAFE runs for rail casks were determined based on a 30,000 gallon fuel spill. A rectangular pool is used to assure the specifications from 10 CFR 71.73 are met in the case of regulatory fires. For consistency the pool remained a square in all other cases. The pool area is 9.25×13.80 m (30.35×45.28 ft) in the Rail-Steel cask configurations, and 9.14×12.42 m (29.99×40.75 ft) in the Rail-Lead cask configurations. These pool areas correspond to a fully-loaded rail tank car burning over a period of 3 hours, the maximum burn time based on 113.6 m<sup>3</sup> (30,000 gallons) of fuel. The pool area is 8.3×12 m (27.2×39.3 ft) in the Truck-DU cask configuration. These pool areas correspond to a fully-loaded, fuel tanker-truck burning over a period of 1 hour, the maximum burn time based on 34.1 m<sup>3</sup> (9000 gallons) of fuel. Only the scenario depicted in Figure IV-1(b), the most severe fire scenario in the analysis of the rail casks, was analyzed for the Truck-DU cask. The pool edges remained 3 m (9.8 ft) away from the surface of the cask in all cask runs.

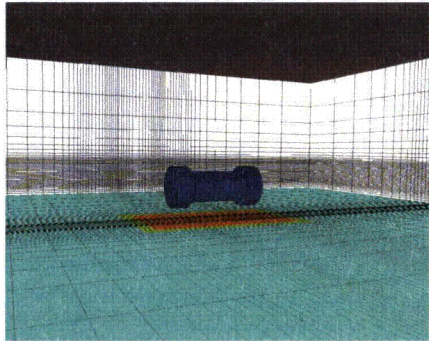
An appropriate domain size is determined from del Valle, et al. (2007) and from del Valle (2009), in which thermal analyses were conducted with CAFE using a calorimeter the size of a rail cask. In these studies, results of CAFE runs are compared to experiments and showed good agreement. In the current study, the ground dimensions varied between cases since a larger domain is required for the cask offset cases, but are at least 25×15×25 m (82×49×82 ft), about the size of the domain used in del Valle et. al. (2007) and del Valle (2009). A mesh refinement study is conducted to assess the sensitivity of the cask external temperatures to mesh size and to determine an appropriate mesh size. Based on this study, a mesh with approximately 90,000 finite volumes was deemed acceptable for both casks. As observed in Figure IV-1, the mesh is finer in the region near the pool. All CAFE scenarios used calm wind conditions; the velocity at the boundaries and inside the domain are originally set to zero, but are allowed to float as the fire develops.

Deleted: s

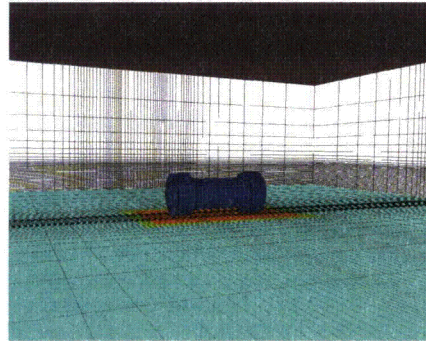
Comment [csb2]: This is confusing as the next few sentences describe rectangular pools.

Comment [csb3]: This discussion bounces back and forth between the rail and truck casks. Can they be separated to make this more coherent?

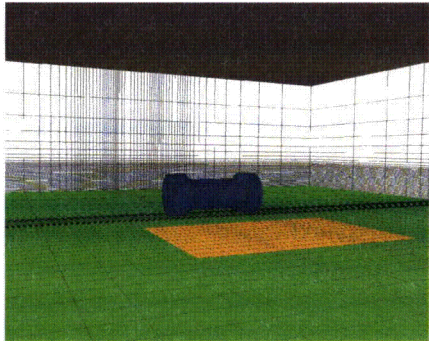
Deleted: this study for



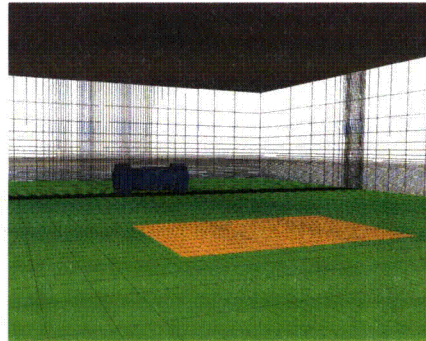
(a)



(b)



(c)



(d)

**Figure IV-1. CAFE three-dimensional domain: (a) CAFE regulatory fire, (b) cask on ground and at the center of the pool, (c) cask on the ground and 3 m (10 ft) from the edge of the pool, (d) cask on the ground and 18.3 m (60 ft) from the edge of the pool.**

### IV.3. The Rail-Steel Cask

The Rail-Steel cask is designed for transportation of a variety of spent fuel assemblies and is intended to fit horizontally on a rail car bed (see Figure IV-2). Therefore, the Rail-Steel cask system is assumed to be in the horizontal position in all CAFE runs (see Figure IV-1), as it would be after derailment if the flatbed rail car overturned or if the cask detached from a rail car after an accident. Only the thermally relevant components of the Rail-Steel cask are considered in this thermal analysis. As stated in the introduction, some results reported in the Rail-Steel cask SAR (Holtec International, 2004) are used in this analysis. Values taken from this report are checked where possible to assess validity of assumptions and to verify results.

Deleted: nuclear

#### IV.3.1 Geometric Consideration

The Rail-Steel cask consists of an overpack, a multipurpose canister (MPC), and two impact limiters; these components fit together as shown in Figure IV-3. The MPC stores the nuclear spent fuel material, and the lid is sealed welded to prevent the contents from leaking into the overpack cavity. The MPC is the first containment barrier in the Rail-Steel cask. The overpack is designed to attenuate both the heat, and the neutron and gamma rays generated inside the MPC. The overpack is secured with a seal to prevent the contents from a breached canister from further leaking into the external environment; thus, the overpack forms the second containment barrier in the Rail-Steel cask. During transportation, the overpack ends are fitted with impact limiters that, besides absorbing most of the impact energy during an impact, add an additional thermal insulation layer to the extreme ends of the overpack.

Deleted: cd

Deleted: tight

Deleted: inner

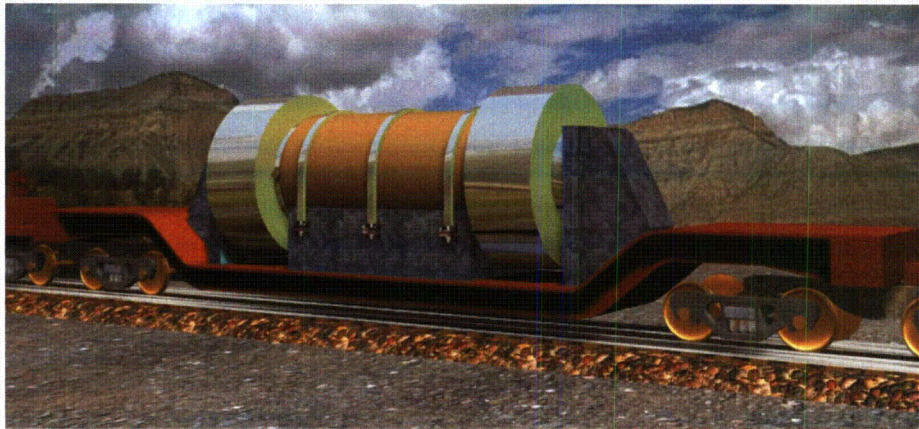
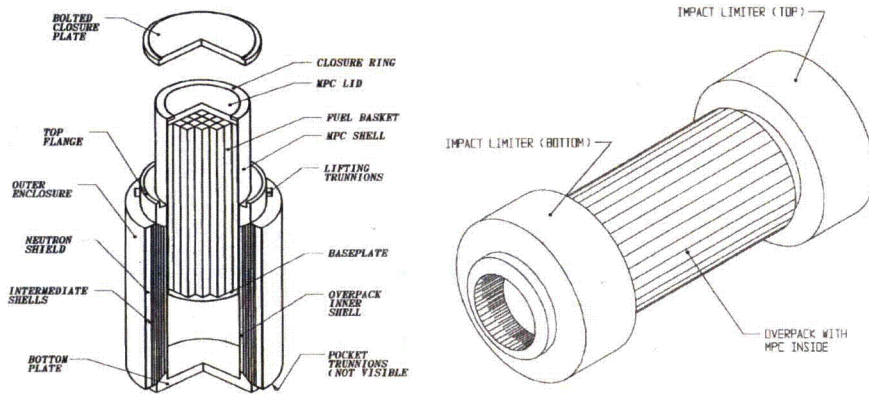


Figure IV-2. Rail-Steel cask transportation system.



(a)

(b)

**Figure IV-3. Rail-Steel cask: (a) assembly of MPC and overpack, and (b) cask with limiters (Holtec 2004).**

#### **IV.3.1.1 The Overpack**

The Rail-Steel overpack is a multilayered cylindrical vessel approximately 2.11 m (83.3 in) in diameter and 5.16 m (203.1 in) in length. The inner cavity of the overpack is approximately 1.75 m (64.7 in) in diameter and 4.85 m (191.1 in) in length. The inner cavity is formed by (1) welding a thick wall cylinder, called the inner shell, to a metal base cup at the bottom and to a large diameter flange at the top, and (2) bolting a closure plate onto the flange as shown in Figure IV-4.

Five thin wall cylinders, tightly fitted to one another and to the inner shell, form the next structural layer of the overpack, strengthening the overpack against puncture or penetration. These cylinders are jointly referred to as the intermediate shells and act as the gamma shield. Channels welded to the outermost intermediate shell extend radially outward and delimit the last layer of the overpack. These channels act as fins enhancing conduction to the periphery of the overpack. Plates welded between the ends of each successive channel complete the outer enclosure shell of the overpack. The cavities formed between the channel walls, and between the outermost intermediate shell and the outer enclosure plates, are filled with a neutron shield material which provides thermal insulation in addition to neutron attenuation. The outermost intermediate shell, the neutron shield region, and the outer enclosure shell effectively extend the diameter of the overpack an additional 32.3 cm (12.7 in) beyond the perimeter of the flange and the metal base cup.

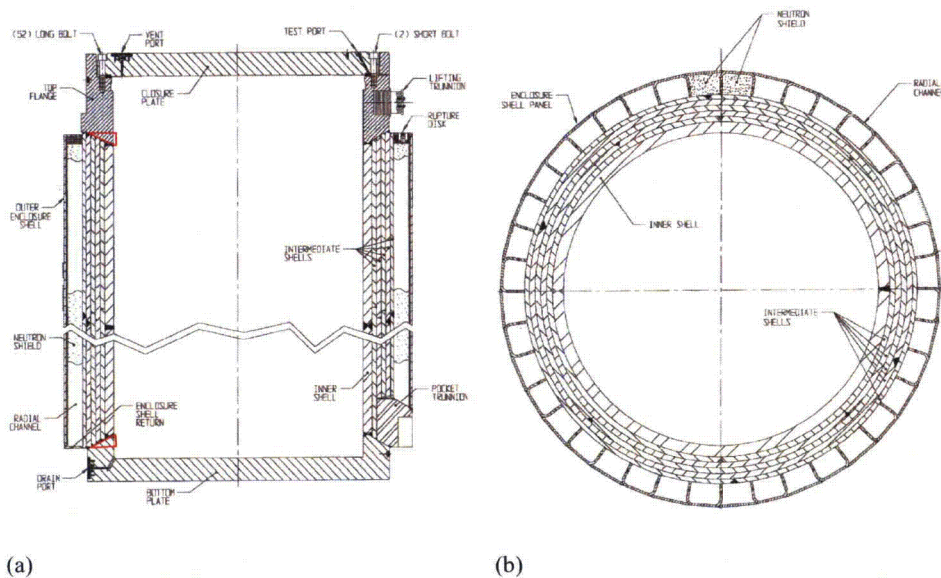


**Figure IV-4. Rail-Steel cask overpack: (a) cross-sectional view through the center of the cask, (b) cross-sectional view through the mid-plane of the overpack (Holtec 2004).**

The overpack shells, metal base cup, flange, closure plate, and neutron shield region are the major components of the overpack and together comprise most of its volume. The overpack shells, metal base cup, flange, and closure plate are represented explicitly in the thermal model with minor alterations to simplify the solid modeling and meshing process. The most significant change is extending the length of the overpack shells to the length of the outer enclosure shell. The regions impacted are outlined in red in Figure IV-4(a). As observed, the regions affected are where the overpack shells meet the metal plate cup and flange. Note that these length change are more pronounced near the inner shell and gradually diminish radially outward. At most, the total length in question is less than 10% of the total length of the outer shell. The materials used for the metal plate cup and flange (cryogenic steel) and the overpack shell (carbon steel) have nearly the same thermal properties. There are contact gap regions between shells that are not present in the metal plate cup and flange. Therefore, these changes are expected to have a limited effect on the overall thermal response of the overpack, but only in the radial direction and limited to the region in question. The intermediate shells and the neutron shield region are each represented as a single volume also to minimize geometric complexity; however, their thermal properties are properly accounted for in the thermal model using the techniques described in Sections IV.3.3.3 and IV.3.3.4.

The overpack contains additional components used to service the overpack during normal operations or designed to function only during abnormal ambient conditions such as fires. These

features include seals, gas ports, rupture disks, and lifting and pocket trunnions as observed in Figure IV-4. These components are not included in the model because their effects are assumed: (1) negligible due to their small volume and mass relative to the other components in the overpack, (2) highly localized with no effect to the overall thermal performance of the cask at locations of interest, or (3) both.

#### IV.3.1.2 Multipurpose Canister

The MPC is a cylindrical vessel approximately 1.73 m (68.3 in) in diameter (outside) and 4.83 m (190.3 in) in length. The MPC is made from a cylindrical shell 1.2 cm (0.5 in) thick and 4.76 m (187.4 in) in length, a circular baseplate 6.35 cm (2.5 in) thick, and a circular plate lid 24.1 cm (9.5 in) thick (see Figure IV-5a). The baseplate is welded to the bottom of the MPC shell, and this shell is in turn welded to the exterior surface of the lid. At the top, the MPC shell is flushed against a large groove on the end perimeter of the circular plate lid. An annular closure ring welded on the groove and to the top of the shell seals the contents of the MPC. In the horizontal position, the shell and the base plate rest on the inner shell of the overpack. Drain and vent ports on the MPC lid are used to evacuate and fill the MPC with an inert gas (generally helium). With the exception of the closure ring and drain ports, all these components are modeled explicitly. The closure ring is assumed to be part of the lid.

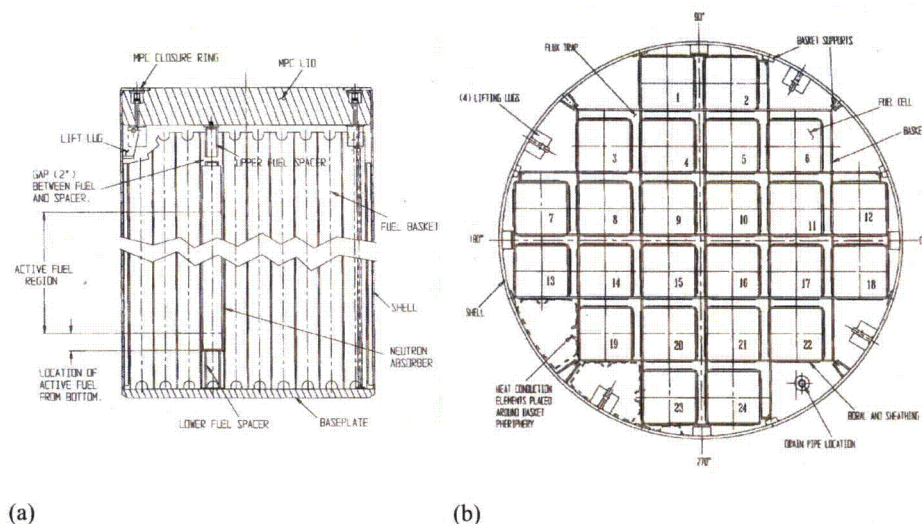


**Figure IV-5. Rail-Steel cask MPC: (a) cross-sectional view through the axis of the cask, (b) cross-sectional through the midplane of the overpack (Holtec, 2004).**

The SNF (or SNF assemblies) is stored in a fuel basket inside the MPC (see Figure IV-5b). The fuel basket is made by welding a series of perpendicular and parallel plates to form an array of storage cells. Each storage cell contains a single fuel assembly. The Rail-Steel cask is designed

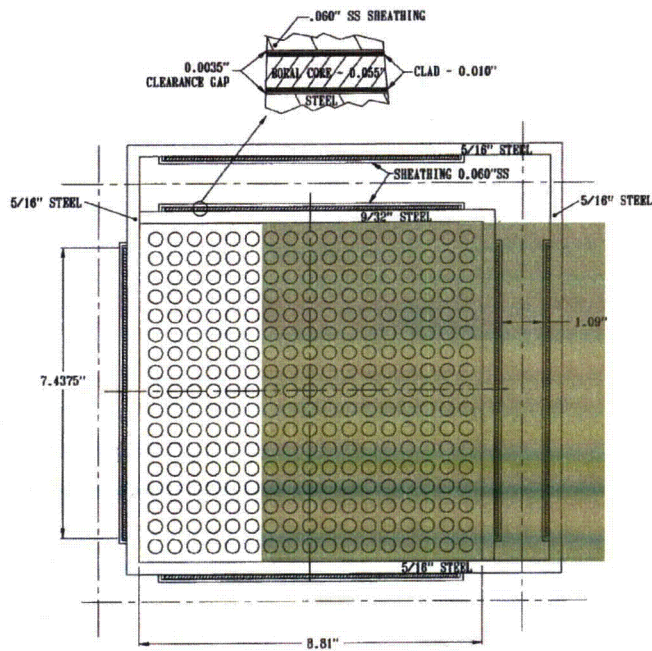
to carry four general types of MPCs: (1) the MPC-24/-24E/-24EF, which contains a maximum of 24 PWR fuel assemblies; (2) the MPC-32, which contains a maximum of 32 PWR fuel assemblies, (3) the MPC-68/-68F, which contains a maximum of 68 BWR assemblies and (4) the MPC-HB, which contains a maximum of 80 Humboldt Bay BWR assemblies. These MPC types are similar in design; however, the MPC-24 is designed to carry a greater specific heat load and the highest total heat load. For this reason, attention is focused on the MPC-24. In the MPC-24, the fuel cells are physically separated from one another by a gas pocket called the flux trap. The length of the fuel basket is approximately 4.48 m (176.5 in). The fuel assembly might not reach this length; in such cases, spacers are installed on the baseplate and on the MPC lid to hold the fuel assemblies in place (see Figure IV-5a).

A single fuel assembly consists of an array of fuel rods, each rod separated by a gas space (when the MPC is backfilled) as shown in Figure IV-6a. The total number of rods per assembly varies with fuel assembly design. Each fuel rod consists of a number of cylindrical fuel pellets fitted into a thin walled pipe, called the fuel cladding. The fuel cladding, inner diameter, is slightly larger than the diameter of the pellets as shown in Figure IV-6b. The fuel pellets are held tightly against each other using the force of a spring. The radial dimensions of the rod components vary between fuel rod designs. In general, the length of the fuel column is only a fraction of the total length of the fuel rod and marks the active fuel region. The total length of the fuel rod is approximately the same as the length of the fuel assembly. Additional supports are added to the ends of the fuel assembly and at regular intervals along the length of the assembly for structural integrity, to maintain spacing between the rods, and for handling purposes.

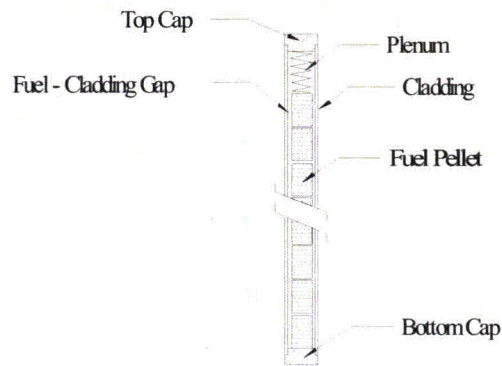
The Rail-Steel cask system is designed to carry a number of PWR fuel rods; it's impractical to analyze the Rail-Steel cask system with all these fuel rod designs. Similarly, it's impractical to model the MPC contents with all the components described above because: (1) the wide range of component length scales creates additional meshing complexities, and (2) alternative methods have been employed in the SAR literature and in this study to obtain equivalent thermal properties for the MPC internal contents with good results (see [Section IV.3.4](#)). Hence, the fuel-basket region, which includes the fuel assembly, basket walls, and flux trap gaps, is not represented explicitly in the Rail-Steel cask model.

**Comment [csb4]:** When printed out, these section numbers appeared as a "0".

The MPC shell contains support structures that help keep the fuel basket laterally in place and lift lugs which are used during loading and unloading operations. Some slots between the periphery of the fuel basket and the MPC shell wall contain thin wall heat conduction elements. These conduction elements extend the full length of the basket and provide an effective heat conduction path between the MPC basket and MPC shell. With the exception of the heat conduction elements, all other structural elements in the fuel-basket periphery region are ignored for the same reason cited in Section IV.3.1.1. The fuel heat conduction elements are not represented explicitly, but their thermal effect is included through the use of a simplified analytical model explained in the Rail-Steel cask SAR.



(a)



(b)

Figure IV-6. Fuel assembly (Holtec, 2004) (a) and fuel rod (b).

To simplify the modeled geometry, the fuel-basket region and fuel-basket periphery region are modeled as two concentric cylindrical regions extending the length of the fuel assembly (see Figure IV-7).

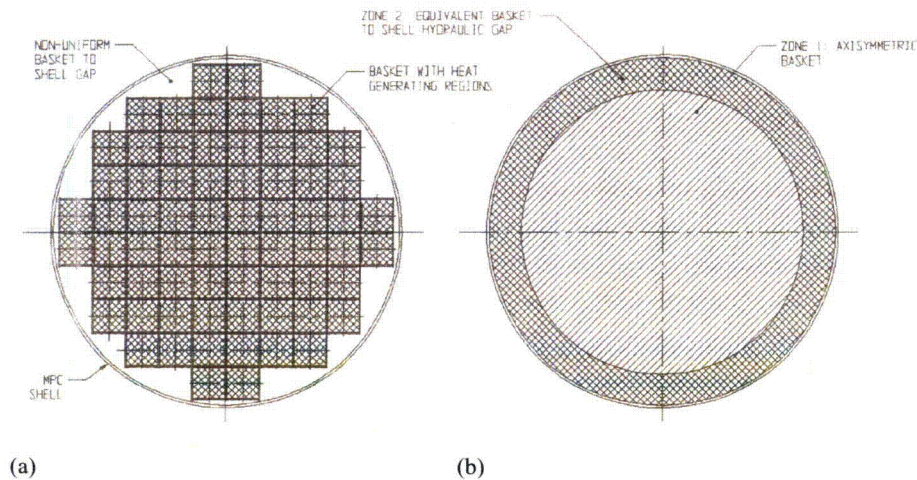


**Figure IV-7. Fuel-basket region (left) and equivalent fuel-basket region (right). (Holtec, 2004).**

The diameter of the equivalent fuel-basket region (Zone 1) is calculated in Holtec International (1997) using the hydraulic diameter of the fuel-basket periphery region (Zone 2). The hydraulic diameter takes into account the perimeter of the fuel basket, MPC support structures, MPC inner shell wall, and the area of the basket-to-shell gap—total surface area between the perimeter of the fuel basket, MPC support structures, and MPC inner wall—through which heat transfer occurs. For the MPC-24 basket, the hydraulic diameter is approximately 12.7 cm (5 in) (Holtec International, 1997). The hydraulic diameter is also equal to the inner diameter of the MPC shell minus the inner diameter of the equivalent fuel-basket cylinder region; in this way, the equivalent fuel-basket cylinder diameter and periphery annulus gap length may be obtained (Zone 2). The periphery annulus gap length obtained from the hydraulic diameter calculation approximates the effective gap length through which heat is transferred between the irregular fuel-basket perimeter, the MPC support structures, and the MPC inner shell wall in the actual cask.

#### **IV.3.1.3 Rail-Steel Cask Impact Limiters**

The impact limiters are relatively low-density cylindrical components that are not only designed to absorb energy during impact but also serve as insulators during fires in the uncrushed state. The main body of the impact limiter has a maximum diameter of 3.25 m (128 in) and a maximum length of 1.52 m (60 in) (see Figure IV-8).

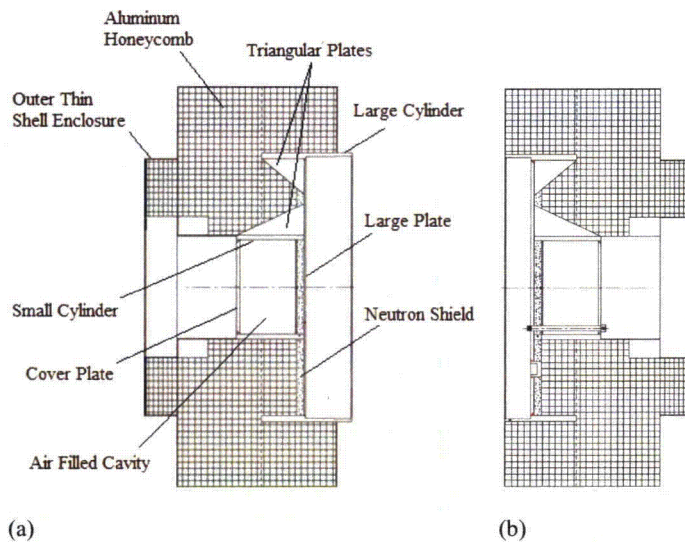


**Figure IV-8. Rail-Steel cask upper (a) and lower (b) impact limiters (Holtec, 2004).**

Most of the impact limiter is honeycomb material enclosed in a thin shell metal wall. The honeycomb material and outer shell walls are supported in the interior of the limiter by a small and a large-diameter cylinder. Both these cylinders are concentric but offset axially from each other. As observed in Figure IV-8, the small cylinder has uniform thickness, but the large cylinder has several wall thicknesses to accommodate the ends of the overpack. The small cylinder has a cover plate at one end and is welded to a large circular plate on the other end. The space inside the small cylinder is filled with air. The large plate is in turn welded to the large cylinder at its perimeter. Triangular plates are welded on one side to the large plate and on the other to the large- or small-diameter cylinders at regular angular intervals (not shown in these views) and complete the support structure in the interior of the impact limiter.

Each impact limiter contains a circular segment of neutron shielding, 6.35 cm (2.5 in) thick, next to the large plate and between the triangular channels. The neutron shield is covered at the other end by a thin shell wall. This neutron shield provides axial neutron attenuation and serves as a heat barrier between the impact limiter body and the overpack ends.

The small and large cylinders extend from one side of the large plate into the interior of the limiter a distance of approximately 54.9 cm (21.6 in) and 34.6 cm (13.5 in), respectively. On the other side of the large plate, the large cylinder extends to the exterior of the limiter, protruding a distance beyond the outer shell only in the upper limiter.

The impact limiters are bolted to ends of the overpack. The upper limiter bolts to the sides of the flange through the protruding section of the large cylinder, and the lower limiter bolts to the

overpack metal base cup through the cover plate, neutron shield, and large plate as shown in Figure IV-8(b).

The impact limiters are assumed to stay intact after the hypothetical accident scenarios described in Chapter 4. This assumption is reasonable since the height of the flatbed rail car is approximately that of the diameter of the overpack. This height precludes any significant damage to the impact limiter during an accident scenario involving, for example, the overturn of the rail car flatbed. Since the limiters are assumed to stay intact, they are modeled in their original shape. The neutron shield material in the limiters is retained, but only up to the surface temperature at which the material starts to degrade (see Section IV.3.3.4). Only the large-diameter, thick-wall, cylinder is explicitly modeled since it serves as a direct conduction path from the exterior to the interior of the limiter.

Deleted: only

### IV.3.2. Rail-Steel Cask Thermal Behavior and Model Assumptions

The MPC-24 is designed to carry a maximum heat load of 20 kW (0.833 kW per fuel assembly). This heat generation rate is non-uniform along the length of the active fuel region. Table IV-1 shows the normalized, axial heat generation rate distribution for a typical Rail-Steel cask PWR assembly (Holtec International, 2004). This table is used in Holtec International (1997) to calculate the heat generation rate through the active length of the basket (i.e., in the axial direction). The Rail-Steel cask system is designed to reject heat passively to the environment under normal conditions of transport. Thus, heat is dissipated from the fuel rods to the exterior surfaces of the cask by a combination of conduction, convection, and radiation heat transfer modes.

**Table IV-1. Axial burn up profile in the active fuel region of the Rail-Steel cask**

Axial Distance from Bottom of Active Fuel(% of Active Fuel Length)	Normalized Value
0% to 4-1/6%	0.548
4-1/6% to 8-1/3%	0.847
8-1/3% to 16-2/3%	1.077
16-2/3% to 33-1/3%	1.105
33-1/3% to 50%	1.098
50% to 66-2/3%	1.079
66-2/3% to 83-1/3%	1.050
83-1/3% to 91-2/3%	0.960
91-2/3% to 95-5/6%	0.734
95-5/6% to 100%	0.467

For normal transportation conditions, the internal temperature is higher than the external temperature of the cask; therefore, heat will be dissipated outwardly starting from the fuel rods. Inside the fuel rods, heat is transferred outward by (1) conduction through the gas space between rods; and (2) by radiation exchange between the fuel rods, and between the fuel rods and the walls of the basket. Convection is assumed negligible in this region since radiation effects dominate at high temperatures. Heat is then dissipated by conduction through the gas space in the flux traps, and by radiation between the basket walls. Convection is also assumed negligible in the flux trap region. In the fuel-basket periphery, heat is dissipated to the MPC shell (1) by conduction through the heat conduction elements and the gas; and (2) by radiation between the walls of the fuel basket and the MPC, and between the inner walls of the heat conduction elements. In this region, natural convection loops enhance heat transfer between the inner walls of the heat conduction elements; this effect is taken into account through the results provided in the Rail-Steel cask SAR. A two-dimensional, finite element model is used to determine the heat convection coefficient for this region of the basket.

Heat transfer from the MPC shell to the overpack inner shell occurs through a MPC-overpack non-concentric gap. In the horizontal position, the MPC makes contact with the overpack at the bottom. This contact gap is approximately 0.5 mm (0.02 in) across. In this region, heat is also dissipated by conduction through the variable gas-filled gap, and by radiation between the outer and inner walls of the MPC and overpack, respectively. A two-dimensional, analytical model is used in the Rail-Steel cask SAR to obtain an effective conductivity through the variable length gap and is discussed in Section IV.3.3.2. Heat transfer through the inner and intermediate shells occurs by conduction through the shell material and through the contact gaps between the shells. These contact gaps are assumed to be five microns (2000  $\mu$ -in) across as in the Rail-Steel cask SAR. Conduction in the neutron shield region occurs in parallel through the radial connectors and the neutron shield material. A simple thermal resistor network is used to calculate the effective thermal conductivity through intermediate shells and through neutron shield region (see Sections IV.3.3.3 and IV.3.3.4).

The Rail-Steel cask system is designed to maintain the temperature of components below their operational temperature limits<sup>1</sup> for normal conditions of transport, and for a 30-minute, fully-engulfing, regulatory fire and subsequent cool down period (10 CFR 71.73). For longer fully-engulfing fires, such as the ones depicted in this study, a significant amount of heat may be transferred to the interior of the Rail-Steel cask, raising the temperature of some of its components above their operational temperature limits. This is expected to occur in the neutron shield region. The operational temperature limit of the neutron shield insulation is 149°C (300°F). In our model, the neutron shield material is assumed to decompose completely shortly after it reaches this temperature limit, immediately triggering thermal radiation exchange between the overpack enclosure shell and the outermost intermediate shell. The assumption used here is a significant departure from what is assumed in the SAR. More will be said in Section IV.3.3 regarding this topic. As with the neutron shield, the aluminum honeycomb is expected to reach temperatures beyond the operational temperature limits. However, the honeycomb material

---

<sup>1</sup> The term operational temperature limit does not necessarily mean melting point. Operational temperature limits are given in the Rail-Steel SAR.

is not expected to completely melt. Given the results in Pierce et al. (2003), the regression rate of the honeycomb material is expected to be minimal over a three-hour period and have only a local effect.

Heat dissipation through the cross section (i.e., in the axial direction) of the MPC and overpack, and through the limiters, is assumed to occur mostly by conduction. Heat conduction occurs in parallel through each of the materials that comprise this cross section. Thermal radiation in the axial direction is possible; however, since view factors tend to diminish with the distance square and angle of view, and the temperature gradients are weak along the axis compared to the radial direction, as observed in contour results presented in Chapter 4, these effects are neglected in the basket region. Thus, radiation effects are assumed to be mostly in the radial direction except near the lateral ends of the MPC. Thermal radiation exchange occurs between the MPC outer surface and the overpack inner lid and between the MPC outer surface and the overpack bottom plate. In the limiters, the thin metal shell covering the neutron shield radiates to the small diameter plate located directly across the air-gap that fills the small diameter cylinder (see Figure IV-8 and the description in Section IV.3.1.3).

With the exception of the contact gaps already mentioned (e.g., between intermediate shell layers and between MPC and overpack), all contact gaps in the Rail-Steel cask are assumed perfect.

### **IV.3.3 Rail-Steel Cask Materials and Thermal Properties**

The Rail-Steel cask system is made from a variety of steel and aluminum alloys. The overpack inner shell is made from SA203-E cryogenic steel, and the metal base cup, flange, and closure plate are made from SA350-LF3 cryogenic steel. The intermediate shells are made from SA516-70 carbon steel, and the radial channels and enclosure plates from SA515-70 carbon steel. The neutron shield material is Holtite-A, a synthetic neutron-absorbing polymer with one percent boron carbide, sold commercially under the trade name NS-4-FR (Holtec International, 2004). The variable-length gap between the MPC and overpack is filled with helium.

The MPC shell, lid, and baseplate; the basket; and the fuel-cell walls are made from alloy X, a generic term used in various SARs that usually stands for one of the following stainless steel metals: SA304, SA304LN, SA316, or SA316LN (Holtec International, 2004). The thermal properties of SA304 are assumed for these components. Very little difference in thermal properties is found between SA304 and the other stainless steel materials already mentioned. On one side of each fuel cell wall is a thin layer of Boral sandwiched between the fuel cell wall and thin stainless steel sheathing. Boral is a neutron absorber made of boron carbide and aluminum alloy 1100 (Holtec International, 2004). The Boral layer and stainless steel sheathing extend the length of the active fuel region. The MPC-24 is designed to carry intact zircaloy and stainless steel clad fuel assemblies. In this study, the fuel rods are assumed to be made from zircaloy cladding as done in the Rail-Steel cask for conservative results. The fuel pellets are uranium dioxide (UO<sub>2</sub>). The MPC heat conduction elements are made from aluminum alloy 1100. All void spaces inside the MPC are filled with helium (Holtec International, 2004).

The honeycomb in the impact limiter is made from aluminum 5052, and the large-diameter cylinder from carbon steel (SA516). The neutron shield segments are also made from Holtite-A.

Table IV-2 provides the thermal conductivity for materials used in the Rail-Steel cask at several temperatures. For aluminum 1100 and the various carbon steels, data from Rail-Steel cask SAR is available only over a limited temperature range since the analysis in that report showed cask temperatures within a limited range due to the limited 30 minute fire exposure and subsequent cool down. For these materials, the data trend is decreasing; therefore, the thermal conductivity value at the highest temperature is used at higher temperatures, a conservative assumption since the thermal conductivity values used are higher than what they should be. Note also that Holtite-A is replaced with air once the temperature of the neutron shield region reached the operational temperature limit of that material. In reality, only a fraction of the Holtite-A decomposes. Some of the gases generated in the shield region outgas through the neutron shield rupture disks at high pressures. Up to 90% of these gases come from moisture in the Holtite-A (Federal Register, 2000). Experiments show that up to 50 percent (by weight) of the NS-4-FR eventually degrades by the time temperature of the material reaches 800°C, leaving behind charred remains (Soo-Haeng, et al., 1996), and these are not expected to combust (Soo-Haeng, et al., 1996; Federal Register, 2000). The thermal conductivity of helium varies with pressure in addition to temperature; however, the pressure dependency is much weaker over the range of 101 to 689 kPa (14 to 100 lb/in<sup>2</sup>) (Petersen, 1970).

**Table IV-2. Thermal conductivities for the Rail-Steel cask materials**

Material	Thermal Conductivity W/m-°C (Btu/ft-hr-°F)				
	92°C (200°F)	226°C (450°F)	377°C (700°F)	477°C (900°F)	726°C (1340°F)
Air <sup>§</sup>	0.026 (0.015)	0.040 (0.023)	0.050 (0.028)	0.055 (0.031)	0.067 (0.038)
Stainless Steel <sup>§</sup>	14.5 (8.3)	18.3 (10.5)	20.4 (11.8)	21.9 (12.6)	25.4 (14.6)
Aluminum Alloy 1100*	228 (131)	212 (122)	—	—	—
Aluminum-Honeycomb <sup>‡</sup>	3.5 (2.0)	4.1 (2.4)	4.8 (2.8)	5.2 (3.0)	—
Boral (B <sub>4</sub> C)*	83.3 (48.2)	83.1 (48.0)	81.3 (47.0)	80.5 (46.5)	—
Carbon Steel- Int. Shells*	42.3 (24.5)	41.7 (24.1)	38.8 (22.4)	—	—
Carbon Steel-N. Shield*	50.7 (29.3)	49.1 (28.4)	42.6 (24.6)	—	—
Cryogenic Steel*	41.1 (23.8)	41.0 (23.7)	38.5 (22.3)	—	—
Helium <sup>§</sup>	0.17	0.22 (0.12)	0.26 (0.15)	0.29 (0.16)	0.35 (0.20)
Holtite-A*	0.65 (0.37)	—	—	—	—
UO <sub>2</sub> *	6.0 (3.4)	6.0 (3.4)	5.1 (2.9)	—	—
Zircaloy*	13.5 (7.8)	14.6 (8.4)	16.2 (9.3)	17.8 (10.2)	—

<sup>§</sup>Incropera and Dewitt, 1996

\*Holtec International, 2004

<sup>‡</sup>Thermophysical Properties Research Laboratory Inc., 2001

Table IV-3 provides the specific heat for these same materials at several temperatures. Temperature dependent values are given only for those materials that exhibited large variation in temperature. With the exception of stainless steel, aluminum 5052, and carbon steel, the specific heat of most materials used in the Rail-Steel cask is fairly constant. Of interest are the properties of carbon steel; the specific heat increases abruptly above 700°C (1292°F) and reaches a peak at around 768°C (1414°F), the Curie temperature. This behavior is associated with changes in the magnetic state of these materials and has been observed for a great number of carbon steel materials (Yafei, 2009). For Holtite-A, limited data is available above its operational temperature limit. Air properties are used beyond this limit. In addition, radiation exchange between the inner and outer surface of the neutron shield region is also allowed above this operational temperature limit to maximize heat input.

**Table IV-3. Specific heat for the Rail-Steel cask materials**

Material	Specific Heat J/kg-°C (Btu/lbm-°F)				
	92°C (200°F)	226°C (450°F)	377°C (700°F)	477°C (900°F)	726°C (1340°F)
Air <sup>s</sup>	1010 (0.24)	—	—	—	—
Stainless Steel <sup>s</sup>	482 (0.11)	535 (0.12)	563 (0.13)	575 (0.13)	611 (0.14)
Aluminum <sup>s</sup>	903 (0.21)	—	—	—	—
Aluminum-Honeycomb <sup>†</sup>	890 (0.21)	976 (0.23)	1057 (0.25)	1100 (0.26)	—
Carbon Steel <sup>s</sup>	434 (0.10)	505 (0.12)	590 (0.14)	653 (0.15)	1169 (0.27)
Boral (B <sub>4</sub> C) <sup>*</sup>	2478 (0.59)	—	—	—	—
Helium <sup>s</sup>	5193 (1.2)	—	—	—	—
Holtite-A <sup>*</sup>	1632 (0.39)	—	—	—	—
UO <sub>2</sub> <sup>*</sup>	234 (0.056)	—	—	—	—
Zircaloy <sup>*</sup>	304 (0.073)	—	—	—	—

Table IV-4 provides densities for stainless steel, carbon steel, zircaloy, and UO<sub>2</sub> at 92°C (200°F), and for air and helium at various temperatures. Since the density of most metals changes very little with temperature, only the values at 92°C (200°F) are used. The density of Holtite-A is assumed not to vary significantly from 92°C to its operational temperature limit. Recall that air properties are used above this limit to replace Holtite-A.

Table IV-5 shows the emissivity values obtained from Rail-Steel cask SAR. The exterior surface of the Rail-Steel cask is coated with Carboline 890 paint and the overpack inner surfaces with Thermaline 450 paints, but these coatings are only good up to 216°C (422°F) and 262°C (505°F), respectively (Holtec International, 2004). Note also the internal surfaces of the heat conduction elements are sandblasted to increase radiation between opposite sides of the heat conduction elements.

**Table IV-4. Densities for the Rail-Steel cask materials**

Material	Density kg/m <sup>3</sup> (lbm/ft <sup>3</sup> )				
	92°C (200°F)	226°C (450°F)	377°C (700°F)	477°C (900°F)	726°C (1340°F)
Air <sup>§</sup>	0.98 (0.061)	0.69 (0.043)	0.54 (0.034)	0.46 (0.029)	0.35 (0.022)
Stainless Steel <sup>§</sup>	7900 (493)	—	—	—	—
Aluminum <sup>§</sup>	2702 (168)	—	—	—	—
Aluminum-Honeycomb <sup>‡</sup>	526 (32)	—	—	—	—
Carbon Steel <sup>§</sup>	7854 (490)	—	—	—	—
Boral (B <sub>4</sub> C) <sup>*</sup>	544 (34)	—	—	—	—
Helium <sup>§</sup>	0.14 (0.008)	0.10 (0.006)	0.077 (0.0048)	0.065 (0.0041)	0.048 (0.003)
Holtite-A <sup>*</sup>	1681 (105)	—	—	—	—
UO <sub>2</sub> <sup>*</sup>	10956 (684)	—	—	—	—
Zircaloy <sup>*</sup>	6551 (409)	—	—	—	—

**Table IV-5. Emissivity for some of the Rail-Steel cask materials and paints**

Material	Emissivity
Zircaloy	0.8
Painted Surface	.85
Rolled Carbon Steel	.66
Stainless Steel	.36
Sandblasted Aluminum	.40

- Formatted: Centered
- Formatted Table
- Formatted: Centered
- Formatted: Centered
- Formatted: Centered
- Formatted: Centered

**IV.3.3.1 Effective Thermal Properties of Fuel Basket and Fuel-basket Periphery**

Thermal properties for the fuel-basket region and fuel-basket periphery are obtained from the Rail-Steel cask SAR. In that report, the fuel basket and the fuel-basket periphery cross sections were replaced with two concentric cylinders, each with equivalent effective thermal properties as described in Section IV.3.1.2. The procedure used to obtain the in-plane thermal conductivities of the fuel basket and fuel-basket periphery as a function of temperature is described in this Rail-Steel cask SAR but is summarized here for completeness.

First, the cross section of the fuel assembly is modeled using a detailed two-dimensional, finite element model of the cross-section of a 17×17 OAF fuel assembly rod arrangement (see Figure IV-7a), a uniform heat generation rate over each fuel rod, and a uniform temperature applied to

the periphery of the fuel assembly. The 17×17OAF assembly used was determined to be the most resistive assembly design (Holtec International, 2004). The finite element model takes into account radiation between the rods and conduction across the helium gap. The effective thermal conductivity is obtained from the following equation:

$$\text{-----}$$

where  $q_g$  is the heat generation rate per fuel cell per unit length,  $a$  is half the length of one side of the fuel cell, and  $\Delta T$  is the maximum temperature difference in the fuel assembly (Sanders et al., 1992). Since radiation is not linearly dependent on temperature, the model is run several times, each time with increasing uniform temperature near on the edge of the fuel assembly, to obtain effective properties at various temperatures. The detail fuel assembly is thus replaced with a homogenized fuel cell region (see Figure IV-7)

Second, the in-plane thermal conductivity of the basket storage wall, Boral, and stainless steel sheathing are replaced with an equivalent thermal conductivity using the thermal resistor network described in the Rail-Steel cask SAR. The representative network takes into account the thermal resistances perpendicular to the wall and along the wall.

Third, the cross section of the MPC is modeled using a two-dimensional, finite element representation of the homogenized, fuel-basket walls, with a uniform heat generation rate applied over each homogenized fuel assembly, and a uniform temperature applied over the perimeter of the MPC shell. The model in the Rail-Steel cask SAR took into account: (1) conduction through the homogenized fuel assemblies, the helium gas in the flux traps, and the basket periphery, (2) radiation between homogenized basket walls, and (3) natural convection loops in the basket periphery. The effective conductivities of the basket region ( $k_b$ ) and periphery region ( $k_p$ ) are given by (Holtec International, 1999):

$$\text{-----}$$

$$\text{-----}$$

where

Here  $q$  is the MPC heat generation per unit length,  $\Delta T_{bm}$  is the maximum temperature difference in the basket,  $\Delta T_{pm}$  is maximum temperature difference in the MPC cross section,  $A_s$  is the surface area per unit length, and  $W$  is basket periphery annular gap length. The equivalent fuel-basket thermal conductivities are given in Table IV-6. The effective axial thermal conductivities of the fuel basket are obtained in the Rail-Steel cask SAR using the resistor method which reduces to an area weighted average since the basket length ( $L$ ) in the resistance ( $L/kA$ ) is equal across all materials. The specific heat and density are obtained using a mass and volume

weighted average, respectively. Near the ends of the basket, the fuel rods are filled with gas, decreasing the in-plane and axial thermal conductivity of the basket slightly, since the thermal conductivity of helium is smaller than the UO<sub>2</sub> pellets. Note that the thermal conductivities vary very little in temperature.

The properties in Table IV-6 are used over the length of the basket. For consistency, temperature varying properties are implemented in the thermal model.

**Table IV-6. Effective thermal conductivity for the fuel-basket region**

Effective Thermal Properties	92°C (200°F)	226°C (450°F)	377°C (700°F)	477°C (900°F)	726°C (1340°F)
In-Plane Thermal Conductivity W/m-°C (Btu/ft-hr-°F)	1.9 (1.1)	2.6 (1.5)	3.4 (1.9)	—	—
Axial Thermal Conductivity W/m-°C (Btu/ft-hr-°F)	3.4 (1.9)	3.8 (2.2)	4.3 (2.5)	4.6 (2.6)	—
Specific Heat J/kg-°C (Btu/lbm-°F)	305 (0.073)				
Density kg/m <sup>3</sup> (lbm/ft <sup>3</sup> )	2688 (168)				

Fuel spacers separate the ends of the fuel assembly from the MPC lid and MPC bottom plate. In these regions, conduction is predominately through the helium gas and through the fuel spacer and fuel basket walls. Thermal radiation also occurs between the walls of the basket and the fuel spacers.

The homogenized material properties used in the fuel spacer region are estimated by taking into account the properties of the fuel region, fuel spacer, the helium, the fuel basket ends, and thermal radiation. A sensitivity study using theoretical bounds indicated the temperatures obtained in the regions of interest were barely influenced by the properties used.

Fourth, the thermal conductivity in the basket periphery is further enhanced to account for heat dissipation through heat conduction elements. The equivalent resistor network through the heat conduction elements is obtained using a two-dimensional, analytical model explained in the Rail-Steel cask SAR. This resistance is added in parallel with the resistance obtained from the two-dimensional, finite element model for the basket periphery region. The fuel-basket periphery, in-plane conductivity is given in Table IV-7.

The axial effective thermal conductivity is obtained from an area weighted average using aluminum 1100 and helium properties. The area of the periphery region is given in Holtec International (1997). The area of the heat conduction elements is estimated at 3.5 times the fuel-basket, cell pitch (27.3 cm [10.7 in]), multiplied by the thickness of the elements (3.175 mm [0.125 in]) and the total number of aluminum inserts (8) (Holtec International, 1999). The specific heat and density of the fuel-basket periphery is obtained from an area and mass weighted average, respectively, again considering only aluminum 1100 and helium.

Heat transfer through the periphery region is further enhanced by radiation between the inner walls of the heat conduction elements and the walls of the MPC and fuel basket. The emissivity of stainless steel and sandblasted aluminum are not very different as observed in Table IV-6.

**Table IV-7. Effective thermal conductivity of the aluminum heat conduction elements**

Effective Thermal Properties	92°C (200°F)	226°C (450°F)	377°C (700°F)	477°C (900°F)	726°C (1340°F)
In-Plane Thermal Conductivity W/m-°C (Btu/ft-hr-°F)	0.43 (0.25)				
Axial Thermal Conductivity W/m-°C (Btu/ft-hr-°F)	10 (5.8)				
Specific Heat J/kg-°C (Btu/lbm-°F)	964 (0.23)				
Density kg/m <sup>3</sup> (lbm/ft <sup>3</sup> )	132 (8.25)				

#### IV.3.3.2 Effective Thermal Properties of MPC-Overpack Helium Gap

In the horizontal position, the MPC rests on the overpack forming a non-concentric, variable-length, helium gap. This gap is not modeled explicitly. Instead, a two-dimensional, analytical model derived in Holtec International (1997) is used to obtain an effective conductivity through the variable-length gap. This model included the effects of the contact region as explained below.

To account for radial heat dissipation through the variable-length, helium gap and through the metal-to-metal contact area, equations for the overall heat conducted through these regions are summed and then equated to the overall heat conducted through a concentric gap to obtain an effective thermal conductivity for a constant-length helium gap (i.e., concentric gap). The following equation taken from the Rail-Steel cask SAR is used to obtain the effective thermal conductivity across the gap ( $k_{gap}$ ):

$$\frac{1}{k_{gap}} = \frac{1}{k_{gas}} + \frac{t}{k_{metal}}$$

where  $k_{gas}$  is the conductivity of the gas,  $t$  is the thickness of the concentric gap and  $\epsilon$  (0.5 mm [0.02 in]) is the metal-to-metal, contact area width. Results reported in the SAR show the effective conductivity through the equivalent concentric gap is twice the conductivity of helium.

#### IV.3.3.3 Effective Thermal Properties of Overpack Intermediate Shells

The Rail-Steel cask consists of a series of shell-gas layers between the inner shell wall and the outermost intermediate shell of the overpack. The contact gaps are assumed to be 0.05 mm (0.002in) across (Holtec International, 2004). No radiation is assumed through these gaps since radiation accounts for less than five percent of the effective conductivity for gaps of this size. The in-plane thermal conductivity is obtained by adding the resistances across each shell and gap

in series (see Table IV-8). The axial and circumferential conductivities are assumed to be that of the shell layer material since the thermal conductivity of air and the gap area of air contribute very little. Similarly, the specific heat and density of the intermediate shell layers are assumed to be equal to the intermediate shell material.

**Table IV-8. Effective thermal conductivity of the intermediate shells in the in-plane directions**

Effective Thermal Properties	92°C (200°F)	226°C (450°F)	377°C (700°F)	477°C (900°F)	726°C (1340°F)
In-Plane Thermal Conductivity W/m-°C (Btu/ft-hr-°F)	13.2 (7.6)	15.6 (9.0)	17.0 (9.8)	18.6 (10.7)	22.1 (12.7)

Formatted: Centered

Formatted Table

#### IV.3.3.4 Effective Thermal Properties of Neutron Shield Region

The neutron shield region consists of the Holtite-A inside the cavities formed between the outermost intermediate shell and the outer enclosure shell, and between the radial channels. Note the outer enclosure shell is not included here since it is modeled explicitly. The neutron shield region includes the Holtite-A material and the radial sections of the channel (2 per channel for a total of 40). This region is also modeled as a single volume with homogenized thermal properties.

Table IV-9 shows the effective properties in the neutron shield region. The effective thermal conductivity in the in-plane and axial direction are obtained by summing the resistance through the radial channels and through the neutron shield material in parallel. Since both the Holtite-A and radial channels extend the same length in the axial direction, the resistance equation in the axial direction reduces to an area weighted average of the individual material conductivities. The effective properties above 300°F were calculated using air in place of Holtite-A and taking into account the radial channels.

**Table IV-9. Effective conductivity of the neutron shield region**

Effective Thermal Properties	92°C (200°F)	226°C (450°F)	377°C (700°F)	477°C (900°F)	726°C (1340°F)
In-Plane Thermal Conductivity W/m-°C (Btu/ft-hr-°F)	4.3 (2.4)	3.5 (2.0)	3.2 (1.8)	3.1 (1.8)	2.7 (1.5)
Axial Thermal Conductivity W/m-°C (Btu/ft-hr-°F)	3.6 (2.0)	3.3 (1.9)	3.0 (1.7)	3.0 (1.7)	2.6 (1.5)
Specific Heat J/kg-°C (Btu/lbm-°F)	1315 (0.31)	505 (0.12)	590 (0.14)	653 (0.15)	1130 (0.28)
Density kg/m <sup>3</sup> (lbm/ft <sup>3</sup> )	2113 (132)	552 (34)			

The thermal conductivity in the circumferential direction is assumed to be that of Holtite-A since the total thickness of the radial channels in this direction is small compared to the total

circumferential length of the Holtite-A. Note that this is a conservative assumption in the sense that heat dissipated through the neutron shield region is preferentially in the in-plane and axial directions as a result of the latter assumption. This assumption does not have an impact in the uniform heating run, but it does have impact on the CAFE-fire runs, where heat input around the circumference of the cask varies. In this case, heat will be dissipated more readily through the in-plane direction; thus giving higher temperatures in the interior of the cask.

The specific heat and density of the neutron shield region are obtained using a mass and area weighted average, respectively. Holtite-A is expected to reach its temperature limit during the early transient period of a fire. When this happens, Holtite-A partially decomposes leaving char residue behind. Most of the excess gas generated in Holtite-A outgases through the rupture disks when the pressure inside the neutron shield region reaches the disks design limits. In the thermal model, when Holtite-A temperature limit is reached, Holtite-A is replaced with air, and radiation is activated by setting the emissivity to an appropriate value. Note that air effectively lowers the specific heat and density of the neutron shield region. The effective specific heat of the neutron shield region is greatly influenced by the specific heat values of carbon steel since the density of air in the mass weighted average is very small compared to carbon steel.

#### **IV.3.4 Rail-Steel Cask, Finite Element Model and Boundary Conditions**

A steady-state case is run to obtain the initial conditions of the Rail-Steel cask and to compare results against those provided in the Rail-Steel SAR and in Adkins et al. (2006). The steady-state model consisted of the Rail-Steel cask being exposed to a 37.8°C (100°F) ambient temperature, radiation boundary condition. This boundary condition is applied over the entire outer surface of the cask using an emissivity of 0.85. In addition, insolation is applied over the outer curved surfaces of the cask (193.8 W/m<sup>2</sup> [61.4 Btu/ft<sup>2</sup>-hr]) and over the flat ends of the cask (96.9 W/m<sup>2</sup> [30.7 Btu/ft<sup>2</sup>-hr]) as specified in the American Society of Testing Materials E 2230 (ASTM, 2008). A convection boundary condition is also applied to the outer surface of the cask using a heat transfer coefficient of 3W/m<sup>2</sup>-°C (0.53 Btu/ft<sup>2</sup>-hr-°F). This value is obtained from a set of correlations described in the Rail-Steel cask SAR—assuming turbulent flow—and is within the same order of magnitude as values obtained from correlations in (Incropera and Dewitt, 1996).

In general, steady-state results are slightly higher than those presented in the Rail-Steel cask SAR, but lower than those reported in Adkins et al. (2006). For example, the current study found a maximum fuel cladding temperature of 376°C (710°F), compared to 372°C (701°F) in the Rail-Steel cask SAR and 392°C (738°F) in Adkins et al. (2006). The largest differences are observed in the extreme ends of the overpack, where temperatures in the Rail-Steel cask are lower (by ~25°C) than reported here and significantly lower (~50°C) than what is reported in Adkins et al. (2006). These differences are attributed to dissimilarities in modeling assumptions and approaches, and boundary conditions. For example, in Adkins et al. (2006), a gap is assumed between the overpack and the limiters. Overall, however, the temperatures obtained from these three studies showed similar spatial trends and good agreement given the differences cited above.

The steady-state case is used to assess the suitability of the mesh. The mesh is initially 169,600 elements; this corresponded to a nominal element size of 10.2 cm (4 in). This value is decreased to 5.1 cm (2 in) and then increased to 15.2 cm (6 in) to study the effects of element size on

temperatures at locations of interest (as shown in the results of Chapter 4 and later in this Appendix). Results of the 15.2 cm (6 in), element-size mesh showed some difference in the temperatures in the interior of the cask when compared to those of the 10.2 cm (4 in), element-size mesh. This is expected since large cells are created in the interior of the cask. Near the exterior of the overpack, small geometric features resulted in small size elements. Results of the 5.1 cm (2 in), element-size mesh showed very little difference when compared to the 10.2 cm (4 in) element mesh. The 5.1 cm (2 in), element-size mesh had smaller elements in the interior and about the same near the exterior of the overpack. Therefore, a third case is run, this time using the 10.2 cm (4 in) mesh, with a refined mesh in the near the exterior of the overpack. Results from this mesh showed some difference (less than 5 degrees in the neutron shield region), but not enough to justify the extra computational time needed to run this mesh. Figure IV-9 shows the final mesh used to run the five scenarios described in Chapter 4.

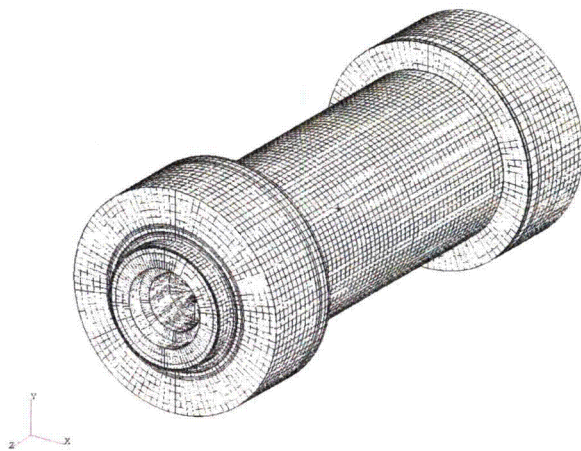


**Figure IV-9. Rail-Steel cask finite element mesh.**

The uniform heating case described in Chapter 4 is run initially to verify the Rail-Steel cask FE model. This exercise gave an additional measure of confidence in the Rail-Steel cask model. The boundary conditions for this case consisted of the Rail-Steel cask being exposed to an 800°C (1472°F) ambient-temperature, radiation boundary condition. This boundary condition is applied over the entire outer surface of the cask using an emissivity of 0.9. A convection boundary condition is also applied to the outer surface of the cask using a heat transfer coefficient of 85W/m<sup>2</sup>-°C (15.2 Btu/ft<sup>2</sup>-hr-°F). This value is obtained in the Rail-Steel cask SAR from a set of correlations described there and assuming a 15 m/s (49 ft/s) vertical flame speed, a value significantly higher than what is specified in Nakos (2005) but nevertheless conservative in that it will result in a higher heat input to the cask. Convection accounts for about 10-20% of the total heat input for large objects inside a fire, the rest is through thermal radiation (Nicolette and Larson, 1989).

The uniform heating case is run for 30 minutes, followed by an 11.5 hour transient cool down with insolation. During the cool down period, the boundary conditions are set back to their steady-state case values, except for the emissivity of the outer cask which remained the same to simulate what happens in actual fires—a blanket of soot covers the cask. Also, unlike the Rail-Steel cask SAR, the neutron shield region is assumed to contain air with radiation interaction between the outer enclosure shell and the outermost intermediate shell.

Overall, maximum temperatures obtained using the model developed here and in the Rail-Steel cask SAR are similar. The difference in purpose of the two analyses leads to some different assumptions, which in turn leads to slightly different results.

For the remaining cases, the external boundary conditions are obtained from CAFE, the computational fluid dynamics code coupled to P-Thermal. As is mentioned in Section IV.2, a boundary condition is setup in PATRAN that allowed CAFE results to be communicated to P-Thermal and vice-versa. The cool down period for these cases also used the steady-state case boundary conditions (from 10 CFR 71.71).

#### **IV.3.5 Rail-Steel Cask Thermal Analysis Results**

Figure IV-10 through Figure IV-14 show results for the five scenarios already described in Chapter 4. These results are not discussed here, but are presented to supplement results discussed in Chapter 4. Figure IV-10 shows results for the regulatory uniform heating case cited in the previous section. This is the P-Thermal only run. Figure IV-11 shows results for the regulatory CAFE fire and together with Figure IV-10 may be useful in determining the differences between uniform and non-uniform fire conditions.

The effect that large objects have on fires and their implications to modeling large casks in fires has been discussed in Nicolette and Larson (1989). Figure IV-12 shows results for the fully engulfing CAFE fire with the cask on the ground, and Figure IV-13 and Figure IV-14 show results for the cask on ground but outside the fire. The last three cases are for a three hour fire and subsequent cool down period.

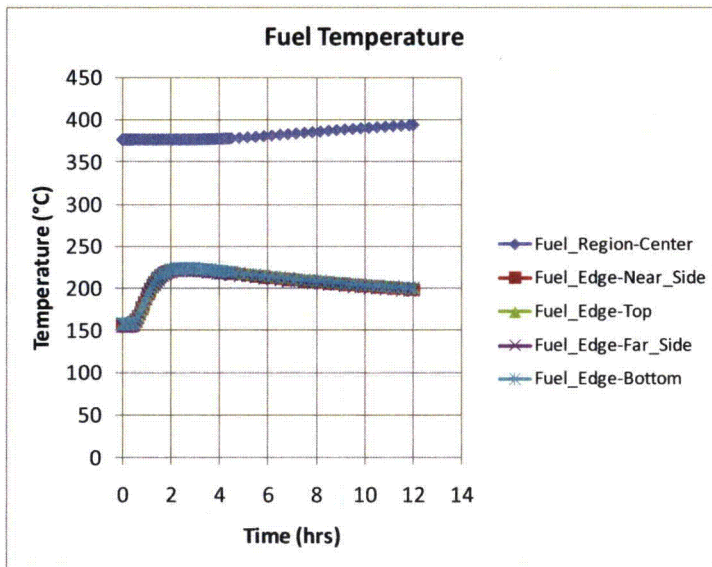
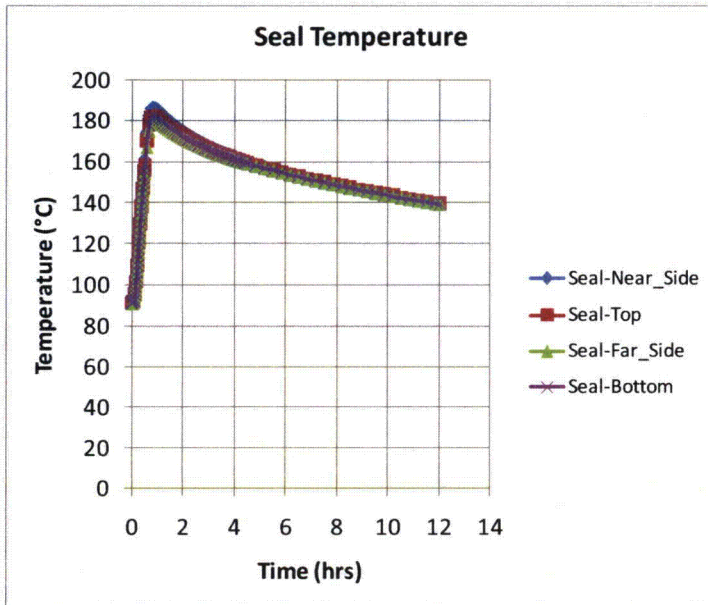


Figure IV-10. Rail-Steel Cask Regulatory Uniform Heating Results (P-Thermal)

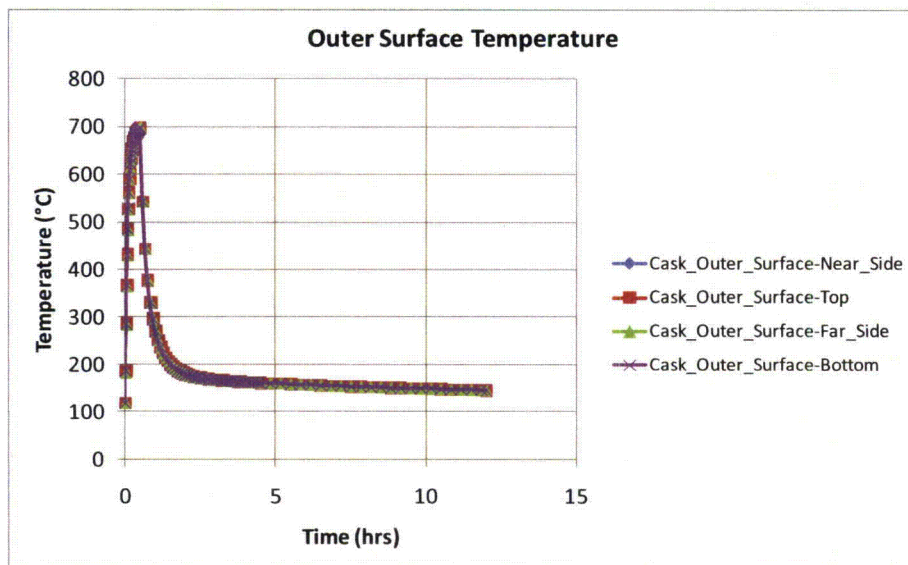
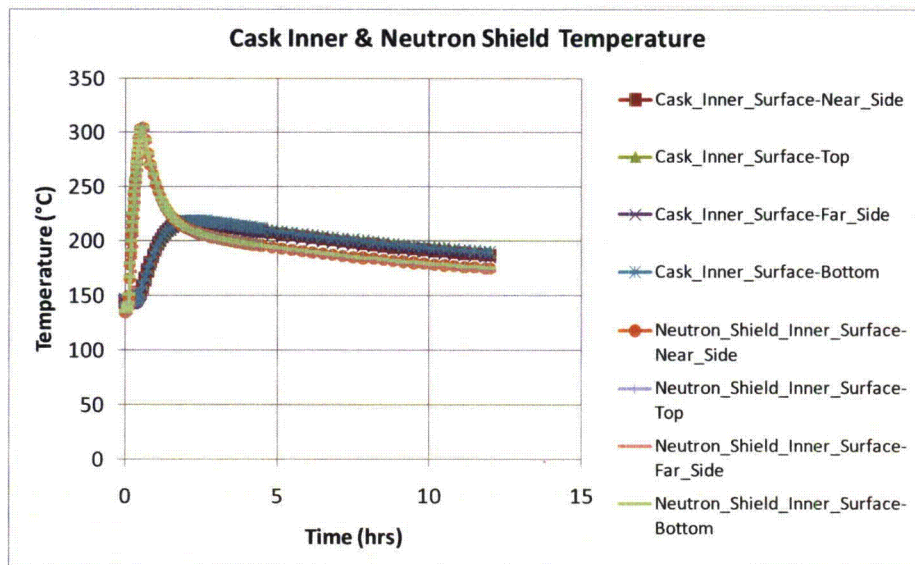


Figure IV-10. Rail-Steel cask regulatory uniform heating results (P-thermal) – continued.

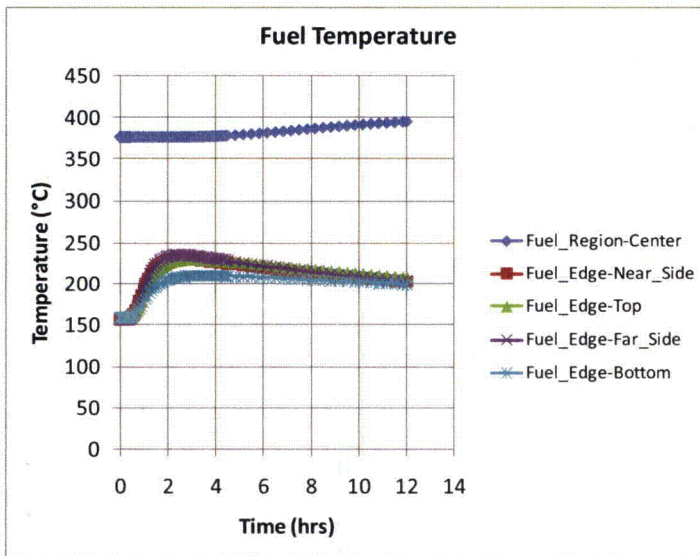
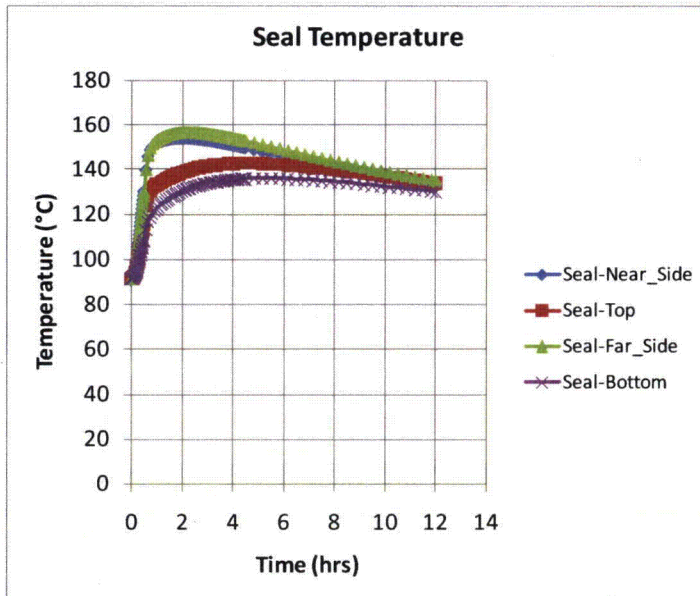


Figure IV-11. Rail-Steel cask CAFE regulatory fire.

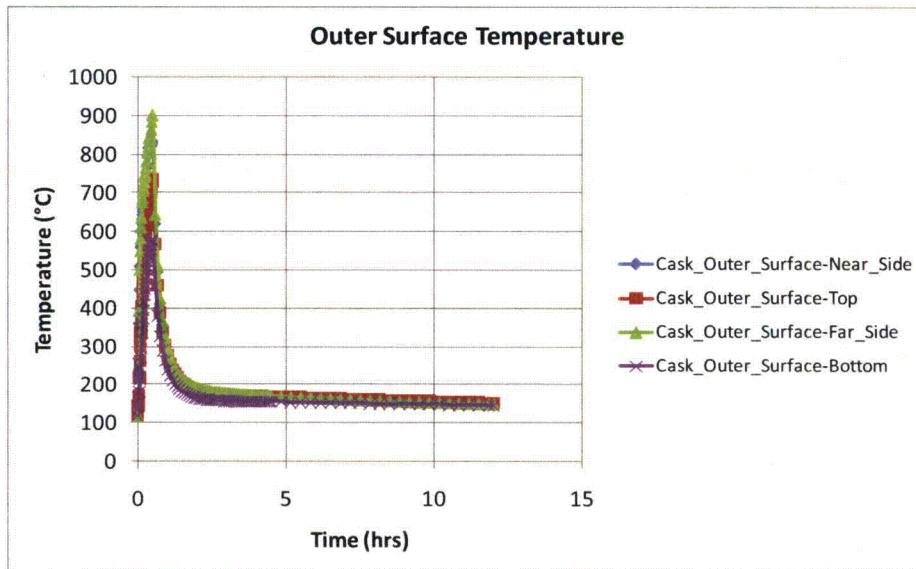
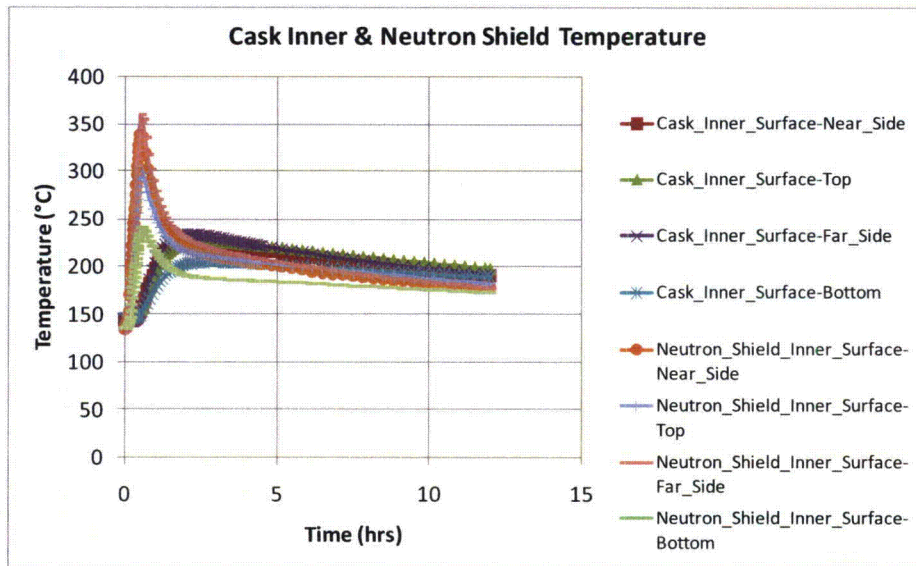


Figure IV-11. Rail-Steel cask CAFE regulatory fire – continued.

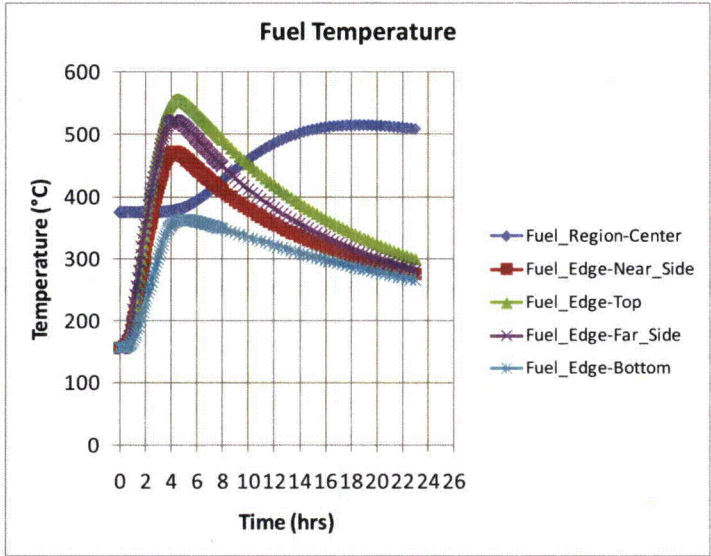
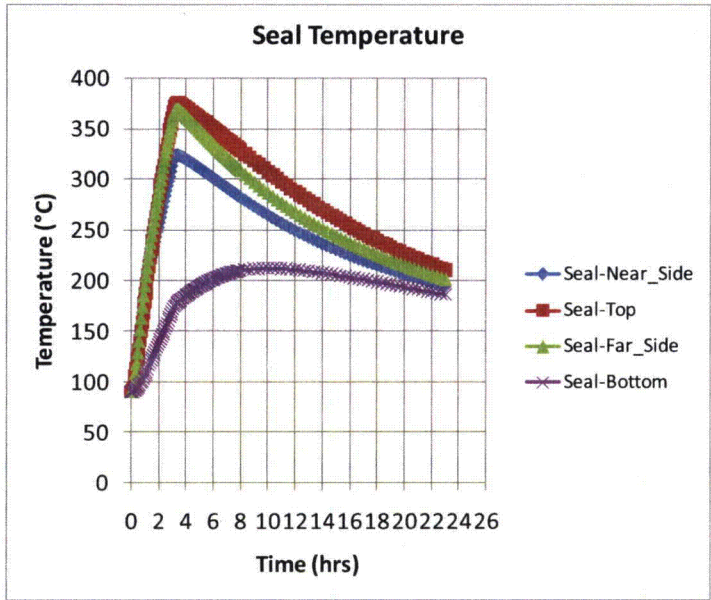


Figure IV-12. Rail-Steel cask CAFE fire with cask on ground and at the pool center.

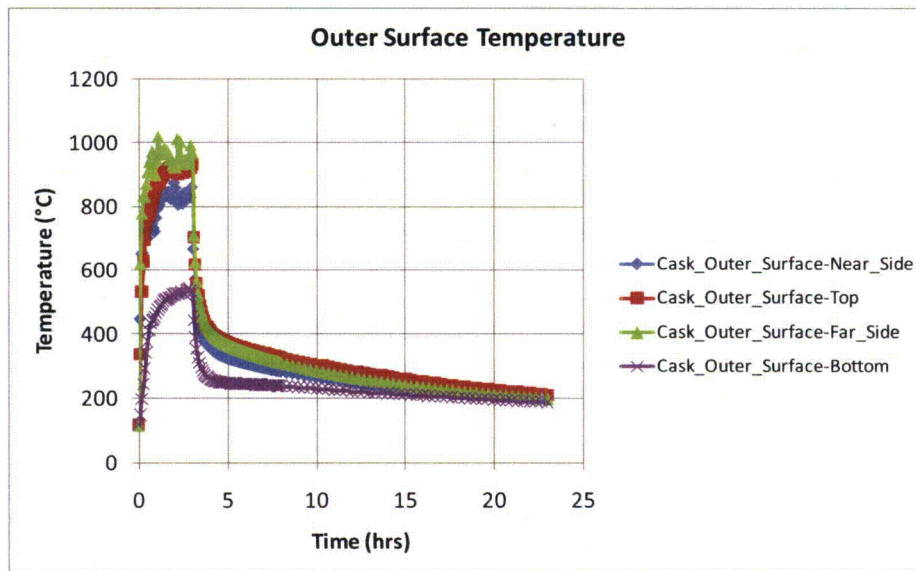
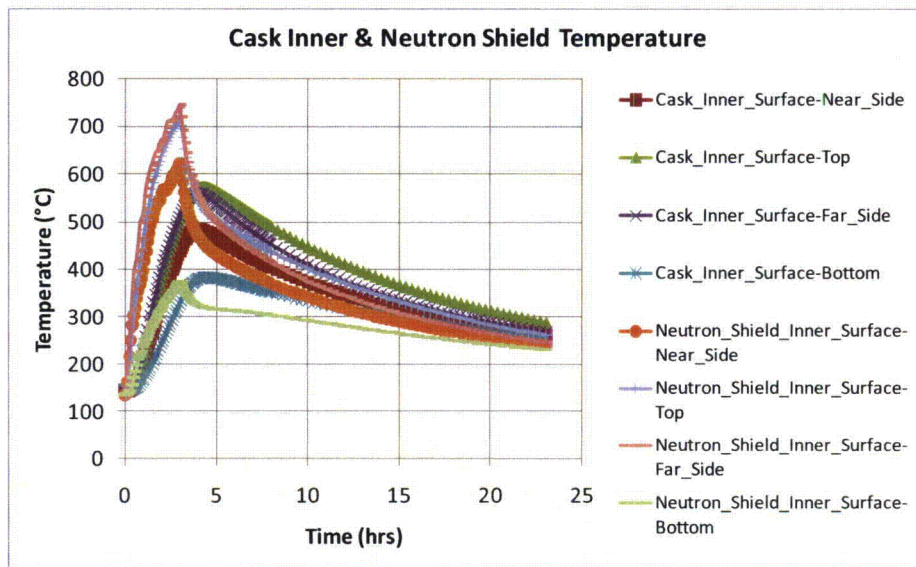


Figure IV-12. Rail-Steel cask CAFE fire with cask on ground and at the pool center – continued

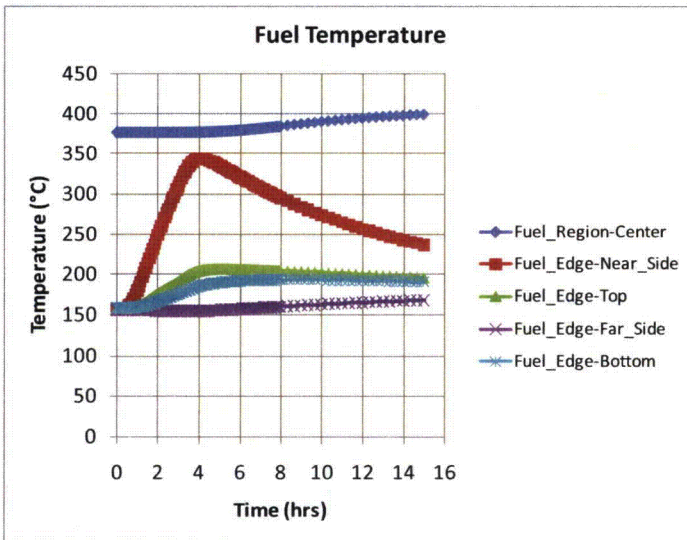
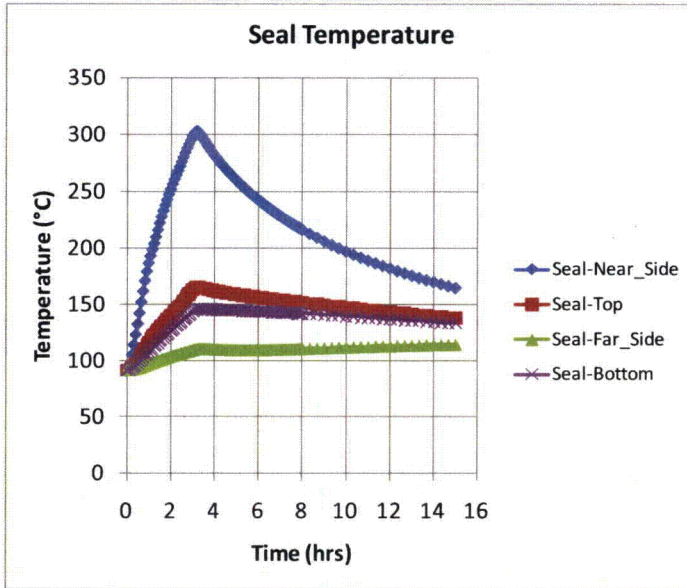


Figure IV-13. Rail-Steel cask CAFE fire with cask on ground 3.0 m (10 ft) from the edge of the pool.

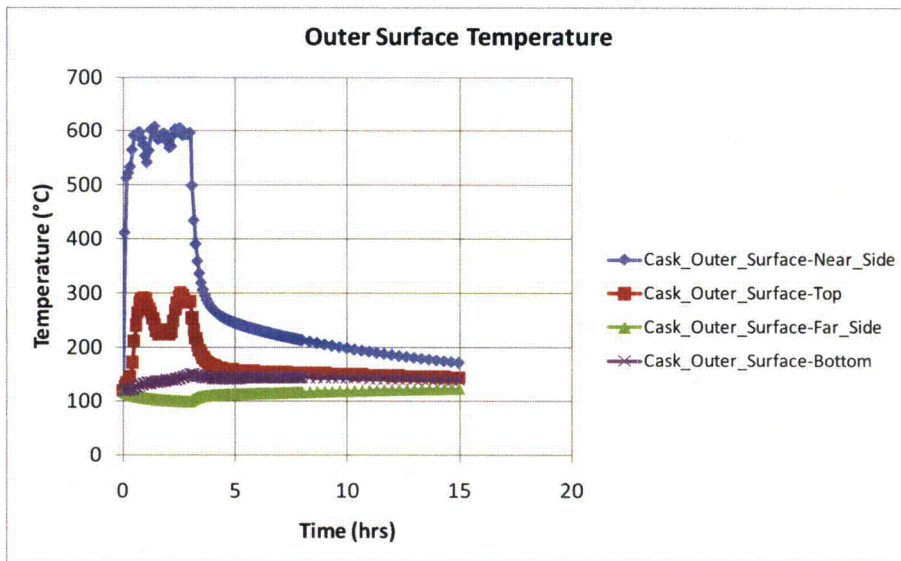
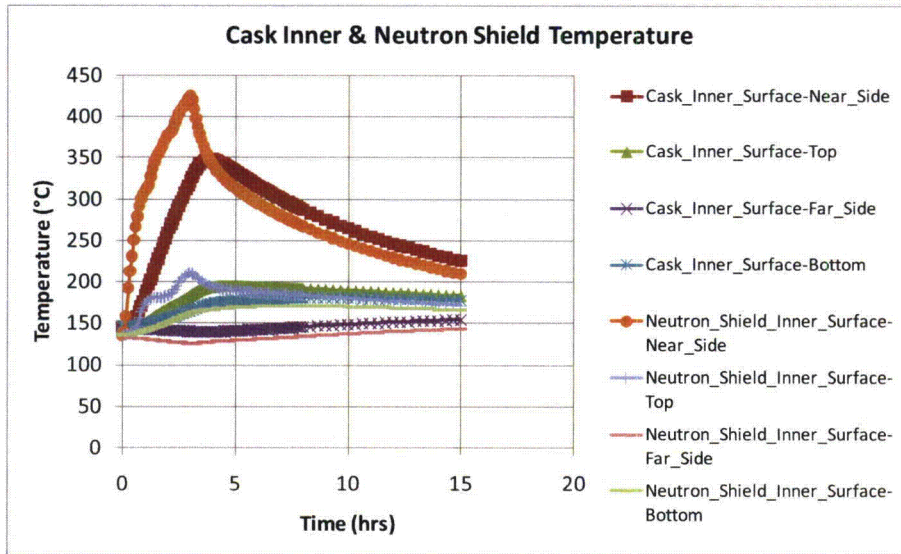


Figure IV-13. Rail-Steel cask CAFE fire with cask on ground 3.0 m (10 ft) from the edge of the pool – continued.

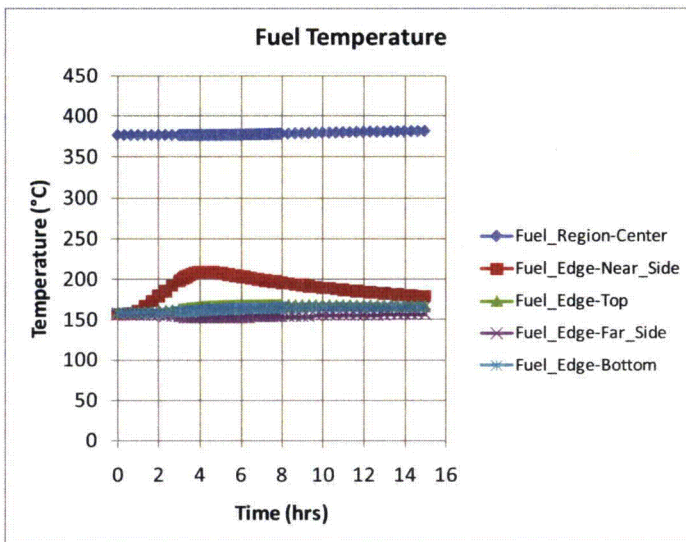
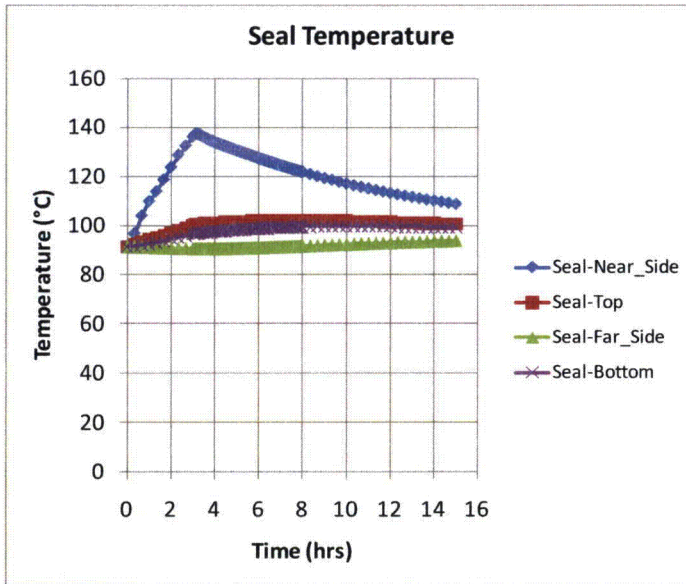


Figure IV-14. Rail-Steel cask CAFE fire with cask on ground 18.3 m (60 ft) from the edge of the pool.

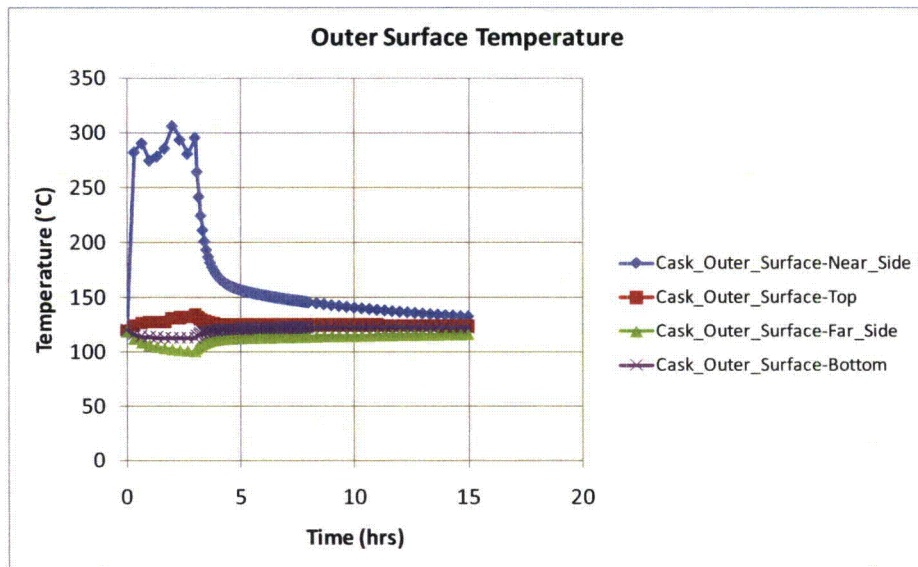
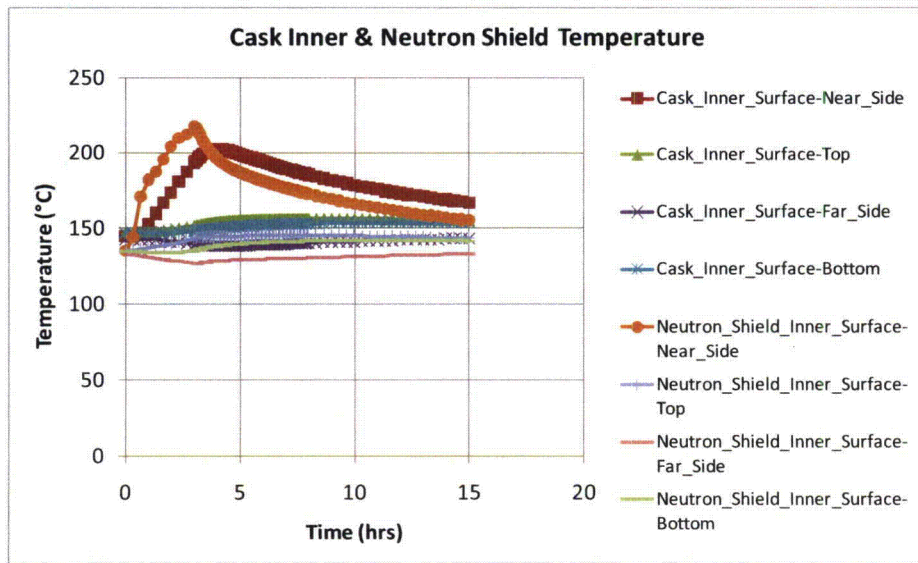


Figure IV-14. Rail-Steel cask CAFE fire with cask on ground 18.3 m (60 ft) from the edge of the pool – continued.

#### **IV.4. Rail Cask with Lead Shielding**

The Rail-Lead cask (NAC International, 2004) is also certified to transport spent nuclear fuel material on rail cars. This cask is chosen because it presents quite a different design philosophy from the Rail-Steel cask. The Rail-Lead cask uses lead for the gamma shield. Moreover, the Rail-Lead cask is certified to carry SNF without a separate canister. As in the Rail-Steel cask analysis, the Rail-Lead cask is assumed to be in the horizontal configuration, as it would be during transportation, and most likely after an accident scenario. Only the thermally relevant components of the Rail-Lead cask are considered to estimate the thermal response of this cask.

The Rail-Lead cask uses a single lead gamma shield as opposed to a multilayer carbon steel gamma shield like the one used in the Rail-Steel cask. This lead shield melts at relatively low temperatures, but remains in the overpack in molten form until the temperature is low enough to change back to the solid state. This process impacts the ability of the cask to attenuate gamma rays as described in Chapter 5 and Appendix V. One unique feature of the Rail-Lead cask is that it can transport the spent nuclear fuel in a directly loaded fuel basket in addition to inside a canister as used in the Rail-Steel cask. The directly loaded configuration is a significant design departure from the MPC configuration since there is no barrier between the fuel assemblies and the inner walls of the overpack. For this reason, this analysis focuses on the directly loaded configuration. Finally, the Rail-Lead cask uses wood filled impact limiters as opposed to an aluminum honeycomb, a minor difference from the thermal analysis point of view, but nevertheless important to point out.

In most cases, results reported in the Rail-Lead cask SAR (NAC International, 2004) are used but modified where necessary as is done with the Rail-Steel cask analysis. The only significant departure is how the interior of the overpack is treated in the Rail-Lead cask SAR, as explained in the introduction of this Appendix. Unlike the method used in that SAR, the directly loaded basket is replaced with a cylinder having equivalent effective thermal properties using a simple, three-dimensional, finite element model and the thermal resistor network method. As is done in the Rail-Steel cask analysis, the neutron shield region is replaced with an equivalent thermal region. The impact limiters are also modeled in the uncrushed state for the same reasons cited in Section IV.3.1.3.

##### **IV.4.1 Geometry Considerations**

The directly loaded Rail-Lead cask consists of an overpack, a fuel basket, and limiters at each end of the basket as shown in Figure IV-15. The directly loaded fuel basket is an open fuel container designed to fit snugly within the overpack interior cavity. The overpack is designed to attenuate both the heat, and the neutron and gamma rays generated inside the fuel basket. The overpack contains two lids, each fitted with seals that completely seal the contents inside the overpack from the outside environment. The total length of the Rail-Lead cask, including the limiters, is approximately 6.5 m (256 in).

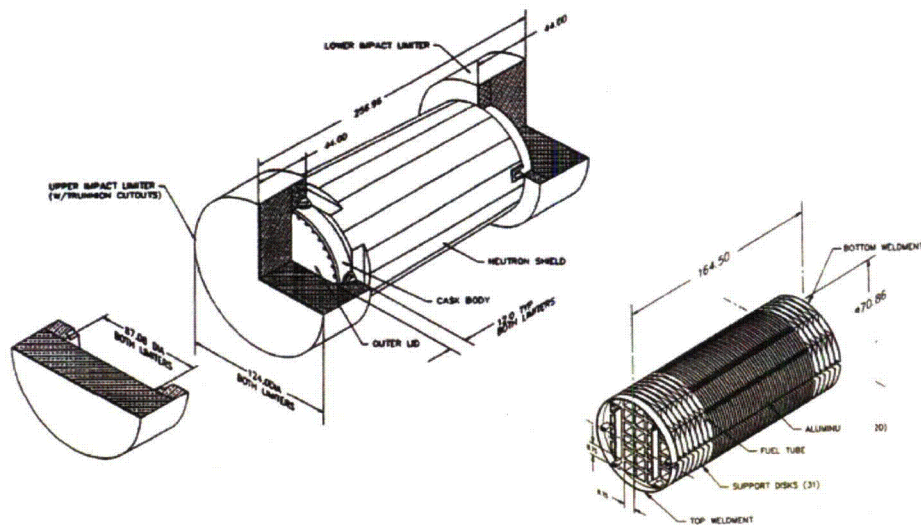
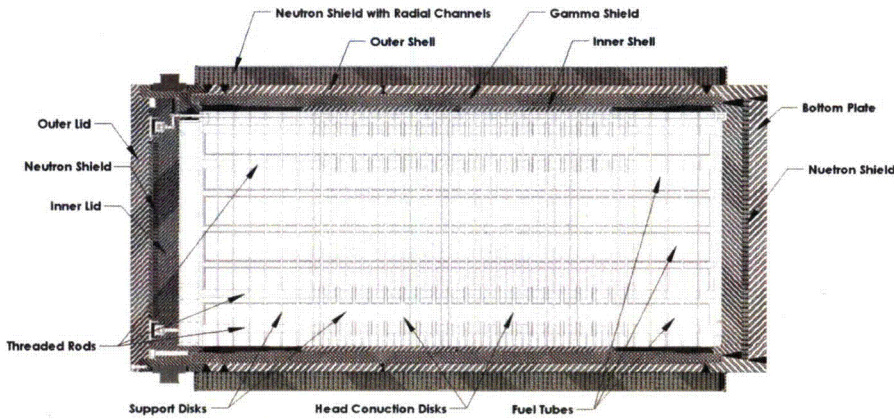


Figure IV-15. Rail-Lead cask components with the direct loaded fuel basket shown to the right (NAC International, 2004).

#### IV.4.1.1 Overpack

The Rail-Lead cask overpack is also a multilayer cylindrical vessel approximately 2.20 m (86.7 in) in diameter and 4.90 m (193 in) in length (see Figure IV-15). The inner cavity of the overpack is approximately 1.80 m (71 in) in diameter and 4.19 m (165 in) in length. The cross section of the overpack vessel is made of three shell layers arranged in following order starting from the center of the overpack: an inner shell, a lead shell, and an outer shell (see Figure IV-16).

As in the Rail-Steel cask, these shells are tightly coupled to each other and are welded to the overpack bottom plate and top flange. The lead shell acts as the gamma shield in this design. The thickness of the inner shell wall is not constant throughout, but tapers in slightly through most of the overpack side wall. That allows the thickness of the lead shell to increase slightly through the same section of the overpack, where the gamma shielding is most needed. Radial channels are also welded to the outer shell to enhance heat transfer through the neutron shield region. The outer enclosure shell is formed the same way as in the Rail-Steel cask. Similarly, the cavities formed by the outer enclosure shell, the radial channels, and the outer enclosure shell are filled with a neutron shield material. The neutron shield region increases the diameter of the overpack an additional 29.2 cm (11.5 in). Unlike the Rail-Steel cask, the overpack contains inner and outer lids that fit into the flange. Both the inner lid and bottom plate contain 5 cm (2 in) thick cylindrical layer of neutron shield within them.



**Figure IV-16. Cross-section view of the Rail-Lead cask with the directly loaded fuel basket.**

The inner, outer, and lead shells, the flange, the inner and outer lids, and the bottom plate are represented explicitly in the thermal model with minor alterations to simplify the model. The most significant change is making the thickness of the inner shell and lead shell constant throughout. Their thickness is kept equal to the corresponding thicknesses in the middle section of the overpack. As in the Rail-Steel cask model, the neutron shield region is represented as a single volume to minimize geometric complexity. As with the Rail-Steel cask, the Rail-Lead cask overpack contains a number of features that serve a special purpose. These features are omitted from the model as is done in the Rail-Steel cask model and for the same reasons: (1) negligible due to their small volume and mass relative to the other components in the overpack, (2) highly localized with no effect to the overall thermal performance of the cask at locations of interest, or (3) both.

#### **IV.4.1.2 Directly Loaded Fuel Basket**

In the Rail-Lead cask, the nuclear spent fuel is stored in a directly loaded basket (see Figure IV-15). In this configuration, the fuel basket can store up to 26 PWR fuel assemblies. The total length of the fuel basket is 4.18 m (164.5 in) and the diameter is a little less than the inner diameter of the overpack. The fuel basket consists of 31 support disks and 20 heat transfer disks, aligned parallel to each other, and each precisely separated using six threaded rods and spacer nuts. The heat transfer disks are placed between the support disks in the region where the heat decay rate is at a maximum. Except for the end support disks, all support disks are the same thickness; the end support disks are twice as thick. Except for the end support disks, all heat transfer disks are slightly thicker. Both disk types contain 26 square holes spaced at regular intervals, and aligned between disks. Each square hole fits a thin walled, square, fuel tube which extends almost the length of the basket. These tubes are welded to the disks and accommodate

the fuel assemblies. The fuel assemblies extend almost the entire length of the fuel basket. The basket active fuel region is assumed to be 3.66 m (144 in) in length as suggested in the Rail-Lead cask SAR. Additional plates and a short length cylinder are welded to the end support disks for extra support and complete the fuel-basket design. The fuel basket fits within the inner cavity of the overpack, but there are a small gap between the basket disks and the inner wall of the overpack, and between the ends of the basket, and the lid and bottom plate walls.

As in the Rail-Steel cask, each fuel assembly consists of an array of fuel rods, each separated by a helium gas space. The total number of rods in the fuel assembly, the dimensions of each rod, and the type of fuel cladding vary between assembly designs. A more complete description of the fuel assembly and fuel rods is given in Section IV.3.1.2.

The fuel basket and fuel assemblies are not explicitly included in the model. Instead, a separate three-dimensional model is generated to obtain the effective properties of the basket in the in-plane and axial directions. Since the basket support disks, gas regions, and heat transfer disks repeat at regular intervals in the active fuel region, a three-dimensional, quarter solid model of a section comprising two support disk, heat transfer disk, and the gas and fuel tubes between them is generated to obtain the effective properties of the basket in the in-plane and axial directions. The diameter of the support and heat transfer disks is assumed the same to simplify the solid modeling and mesh process. The same model is used for the portion of the fuel basket without the heat transfer disk. In this case, the material properties and boundary conditions for the heat transfer disk are replaced with those of the gas region.

#### **IV.4.1.3 Impact Limiters**

The impact limiters in the Rail-Lead cask are cylindrical wood-filled structures also encased in a thin metal shell. Each impact limiter is 3.15m (124in) in diameter and 1.12m (44in) in length (see Figure IV-15). The depth of the cap where the overpack fits is 30.5cm (12in). These limiters serve the same purpose as the impact limiters in the Rail-Steel cask (see Section IV.3.1.3). Since the impact limiters are mostly wood and have very little metal as part of their structures, they are modeled as two coupled solid wood structures, retaining their volume and shape.

Deleted:

#### **IV.4.2 Rail-Lead Cask Thermal Behavior and Model Assumptions**

The Rail-Lead cask is also designed to release heat passively under normal conditions of transport. In the direct loaded configuration, the basket is designed to accommodate a maximum heat load of 22.1 kW (0.85 kW per fuel assembly). Figure IV-17 shows the normalized, axial heat generation rate distribution for a 0.85 kW PWR assembly. As with the Rail-Steel cask, heat is dissipated from the fuel rods to the exterior surfaces of the Rail-Lead cask by a combination of conduction, convection, and radiation heat transfer.

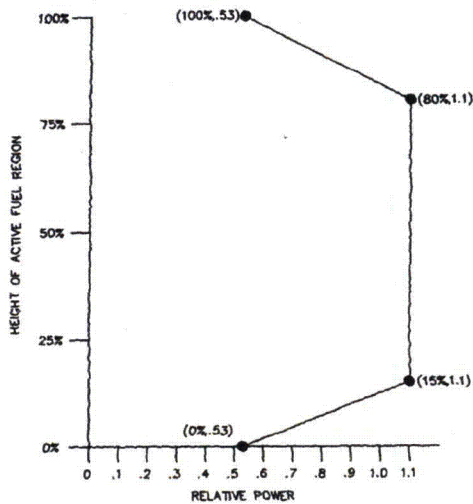


**Figure IV-17. Axial burn up profile for the directly loaded fuel basket (NAC International, 2004).**

The fuel assembly design in the Rail-Lead cask is conceptually the same as in the Rail-Steel cask model; therefore, the same heat transfer mechanisms are present as described in Section IV.3.2. The approach described in Section IV.3.3.1 is also used in the Rail-Lead cask SAR to obtain the effective thermal conductivity of the fuel assembly in the radial direction. Values presented in the Rail-Lead cask SAR are used in this study and are not much different from what is used in the Rail-Steel cask SAR, as expected. Heat generated in the assembly is dissipated by conduction through the fuel tube walls. From the tubes, heat is then radially dissipated by conduction through the support and heat transfer disks, and through the gas in the void formed between the tubes and the inner wall of the overpack; and by radiation to the adjacent tubes and disks, and to the inner wall of the overpack. As in the Rail-Steel cask fuel basket, convection is limited to a few regions around the basket perimeter. However, unlike the HI-STAR configuration, the convective cells in the Rail-Lead cask fuel basket are confined to the gas void between adjacent disks. Moreover, heat dissipated from the adjacent disks through this void tends to decrease the temperature gradient across this void region, reducing temperature gradient induced flow. In the Rail-Lead cask model, convection is neglected in this region since it is not expected to be significant given the Nusselt values presented in the Rail-Steel cask SAR for a similar void configuration.

Heat is dissipated radially by conduction and radiation through the gap between the disks and the overpack inner wall. This gap is assumed to be 1.65 mm (0.065 in) across as stated in the Rail-Lead cask SAR. As mentioned before, a three-dimensional, quarter section of the fuel basket is generated to obtain effective thermal conductivities in the in-plane and axial directions (see

Figure IV-18). The small gap between the disks and the inner wall of the overpack is included (not visible in Figure IV-18). Except for convection, all modes of heat transfer are accounted for in this model, and included radiation between the tubes, between the tubes and the disks, between the tubes and the inner shell (also not shown), between the disks, and between the disks and the inner shell. In the horizontal position, the disks make contact with the inner shell wall. To account for conduction through the contact area between the disks and the inner shell wall, the same model derived in Holtec International (1997) is employed to enhance conductivity through the equivalent concentric gap (see Section IV.3.3.2). Note that both the support and heat transfer disk diameters are assumed to be the same after thermal expansion.

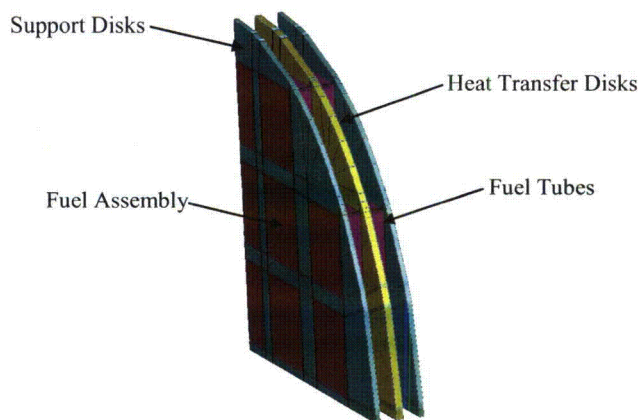


**Figure IV-18. Three-dimension, quarter section of the directly loaded basket. The helium material is not shown.**

Heat transfer through the inner shell, lead, and outer shell of the overpack occurs by conduction through the shell materials. These are modeled explicitly. As in the Rail-Steel cask, conduction in the neutron shield region occurs in parallel through the radial connectors and the neutron shield material.

Heat transfer from the cross section of the direct loaded basket and overpack to the axial ends of the overpack is assumed to occur by conduction and radiation. Heat conduction occurs in parallel through each of the connecting materials that comprise the basket and overpack. The effective thermal properties are obtained in the same manner as in the Rail-Steel cask model. Radiation is assumed to occur between the end disks of the basket to the interior wall of the inner lid and bottom plate of the overpack.

The Rail-Lead cask system is also designed to maintain the temperature of critical components below their design limits during and after a 30 minute, fully engulfing, hypothetical accident condition (HAC) scenario. For fire accident scenarios lasting longer than the HAC fire described in 10 CFR 71.73, a significant amount of heat may be transferred to the interior of the cask. As in

the Rail-Steel cask, the temperature of the neutron shield is expected to reach temperatures beyond its material temperature limits. Heat then is dissipated by conduction through the gas layer in the neutron shield and by radiation between the outer wall of the intermediate shell layer and the outer enclosure shell. Similarly, the lead shell is expected to melt since its melting point is around 321°C (611°F). The impact limiters are made of wood encased in a thin metal layer and are sealed to prevent moisture from deteriorating the wood over long periods of time. Since the impact limiters are assumed to stay intact (i.e., with the content sealed) after the initial accident event (e.g., derailment), the wood is not expected to char significantly. Charring is therefore not taken into account in this model.

#### IV.4.3 Rail-Lead Cask Materials and Thermal Properties

The Rail-Lead cask is made of stainless steel, lead, copper, aluminum, NS-4-FR, and Boral neutron absorber, and is backfilled with helium. The inner and outer shell, the outer enclosure shell, the bottom plate, the top flange, and the inner lid of the overpack are made from stainless steel, type 304. The gamma shield is made from copper-lead, and the outer lid from stainless steel, type 630. The radial channels are made from a combination of stainless steel, type 304, copper, and a small section of carbon steel. The stainless steel in the channel serves as the main support component, while the copper enhances conduction through the channels. The overpack neutron shield is made from NS-4-FR. The impact limiters are redwood and balsa layers encased in a thin stainless steel shell.

In the fuel basket, the support disks, threaded rods, and spacer nuts are made from stainless steel, type 630, and the top and bottom support plates, short length cylinder, and fuel tubes from stainless steel, type 304. The heat transfer support disks are made from aluminum alloy 6061. As with the Rail-Steel cask, adjacent to each fuel tube wall is a layer of Boral sandwiched between the tube wall and a thin layer of stainless steel sheathing. The fuel rods are assumed to be zircaloy as in the Rail-Steel cask analysis. The pellets are made from UO<sub>2</sub>. The empty gas space, which encompasses most of the volume inside the overpack cavity, is filled with helium.

Table IV-10 through Table IV-13 provide the thermal conductivity, specific heat, density, and emissivity for those materials used in the Rail-Lead cask which are different from the Rail-Steel cask, or for which the properties are significantly different (see Table IV-2 through Table IV-5 for additional properties). The properties of NS-4-FR reported in the Rail-Lead cask SAR are marginally different from those reported for Holite-A, as expected. The thermal conductivity of redwood and balsa vary depending on the direction of the grain. For balsa, values from MSC Patran material database are used and compared well with values in Incropera and Dewitt (1996). The MSC Patran database references are given in Table IV-10. NUREG-0361 (NRC 1978) gives values through and along the grain for redwood; however, since the Rail-Lead cask SAR does not specifically describe the arrangement of the wood layers in the limiters, average properties (along and through the grain) are assumed. The specific heat and density of copper-lead provided in the Rail-Lead cask SAR are slightly lower and higher, respectively, than for plain lead (Incropera and Dewitt, 1996); properties from MSC Patran database are used instead since data is readily available above the melting temperature and includes the specific latent heat of fusion (23.9 kJ/kg [10.3 Btu/lbm]). The specific heat of lead increases up to the melting point (by a

factor of 1.07), but then remains approximately the same. Since these changes are small, the value at 92°C is used throughout the rest of the temperature range.

**Table IV-10. Thermal conductivities for the Rail-Lead cask materials**

Material	Thermal Conductivity W/m-°C (Btu/ft-hr-°F)				
	92°C (200°F)	226°C (450°F)	377°C (700°F)	477°C (900°F)	726°C (1340°F)
Aluminum 6061*	171 (98.8)	176 (101.7)	176 (101.7)		
Copper <sup>§</sup>	402 (232.4)	386 (223.1)	376 (217.3)	369 (213.3)	352 (203.5)
Balsa <sup>¶</sup>	0.050 (0.029)	—	—	—	—
Lead <sup>‡</sup>	33.9 (19.6)	29.3 (16.9)	16.7 (9.7)	15.3 (8.8)	14.7 (8.5)
Redwood <sup>¶</sup>	3.6 (2.0)	5.5 (3.1)	—	—	—
Stainless Steel Type	17.5 (9.9)	18.3 (10.6)	20.7 (12.0)	24.6 (14.2)	—

\*Nuclear Acceptance Corporation International, 2004

<sup>§</sup>Incropera and Dewitt, 1996

<sup>¶</sup>McAdams, 1954; Perry, 1963; Weast, 1966

<sup>‡</sup>Kelley, 1960; Schorsch, 1966; Weast, 1966

<sup>¶</sup>NUREG-0361, 1978

**Table IV-11. Specific heat for the Rail-Lead cask materials**

Material	Specific Heat J/kg-K (Btu/lbm-F)				
	92°C (200°F)	226°C (450°F)	377°C (700°F)	477°C (900°F)	726°C (1340°F)
Copper <sup>§</sup>	390 (0.093)	406 (0.097)	422 (0.101)	431 (0.103)	451 (0.108)
Balsa <sup>¶</sup>	2302 (0.55)	—	—	—	—
Lead <sup>‡</sup>	131 (0.031)	—	—	—	—
Redwood <sup>¶</sup>	2386 (0.57)	3898 (0.93)	—	—	—

**Table IV-12. Densities for the Rail-Lead cask materials**

Material	Density kg/m <sup>3</sup> (lbm/ft <sup>3</sup> )				
	92°C (200°F)	226°C (450°F)	377°C (700°F)	477°C (900°F)	726°C (1340°F)
Aluminum 6061 <sup>*</sup>	2823 (176)	—	—	—	—
Copper <sup>s</sup>	8933 (558)	—	—	—	—
Balsa <sup>y</sup>	130 (8.1)	—	—	—	—
Lead <sup>z</sup>	11350 (709)	—	—	—	—
Redwood <sup>c</sup>	352 (22)	—	—	—	—

**Table IV-13. Emissivity for some of the Rail-Lead cask materials**

Material	Emissivity
Aluminum 6061	0.22
Stainless Steel Type 630	0.58

With the exception of the basket and neutron region, all components are modeled explicitly. The impact limiters are modeled in their intact state, with properties of redwood and balsa, since the outer shell volume is significantly smaller than the total wood volume. Contact gap effects are assumed negligible. As in the Rail-Steel cask model, NS-4-FR is replaced with air when the former reached its temperature limit, but only in the neutron shield region of the overpack. Radiation is activated in this region by setting the emissivity to the appropriate value.

#### **IV.4.3.1 Directly Fuel Loaded Basket**

In the Rail-Lead cask SAR, fuel rods are evaluated to determine a representative fuel rod configuration. The fuel assembly is then modeled explicitly to obtain an equivalent in-plane thermal conductivity for the homogenized fuel assembly, as described in Section IV.3.3.1. The fuel assembly axial conductivity is next obtained with an area weighted average using the thermal conductivities of the individual components of the fuel rods and helium. The rest of the directly loaded basket with the homogenized fuel assembly is then included explicitly in the normal condition run, but is not included in the subsequent regulatory fire accident run. Instead, the maximum temperature difference between the fuel basket and the inner wall of the overpack calculated in the normal condition run is added to the inner wall temperature of the overpack calculated in the regulatory fire run to obtain an estimate of the temperature of the center of the fuel basket for the regulatory run. Since homogenized properties for the fuel basket region were not provided in the Rail-Lead cask SAR, a different approach is used in this study to obtain these properties. This alternate approach (1) reduces geometric modeling complexities while maintaining the overall response of the cask and (2) is consistent with the approach employed to model the Rail-Steel cask.

The directly loaded fuel basket is replaced with a homogenized cylinder having equivalent effective thermal conductivities in the in-plane and axial directions. As described in Section IV.4.2, two variations of the same three-dimensional, quarter section, finite element model are generated. The first model included two support disks, a heat transfer disk, and the fuel tubes and helium space between the disks (see Figure IV-18). The second model did not include the heat transfer disk; instead, it is replaced with helium and the boundary conditions are modified to reflect this change.

Since the effective in-plane and axial conductivities for the fuel basket are not explicitly given in the Rail-Lead cask SAR (i.e., the fuel basket was modeled explicitly in that SAR), these effective conductivities are obtained using the following four-step procedure.

*First*, the detail cross section of the fuel assembly is replaced with a homogenized fuel region having equivalent thermal properties. This analysis is done in the Rail-Lead cask SAR, as explained above, and the analysis results are included in this study. As expected, the thermal conductivities reported in the Rail-Lead cask SAR are close to those reported in Rail-Steel cask SAR for similar fuel assemblies, which serves as a check. *Second*, the fuel tube, Boral, and stainless steel sheathing are replaced with a homogenized wall having an equivalent thermal conductivity as described in the Rail-Lead cask SAR.

**Comment [csb5]:** You should use italics for the previous section where you had items 1 to 4 (First through Fourth) to be consistent.

*Third*, both three-dimensional, quarter section models described above (and shown in Figure IV-18) are used to obtain the in-plane and axial effective thermal conductivities. Each model is evaluated with two sets of boundary conditions:

- (1) a uniform temperature applied over the outer circumference of the inner shell, adiabatic conditions over the in-plane ends, and uniform heat generation in the homogenized fuel assemblies; and
- (2) adiabatic conditions applied over the outer circumference of the inner shell, a uniform temperature over one of the in-plane ends and a uniform heat flux over the other in-plane end, and no uniform heat generation in the homogenized fuel assemblies.

In the first case, the in-plane thermal conductivity is obtained using the same procedure described in Section IV.3.3.1. In the second case, the axial thermal conductivity is obtained using the standard relationship:

---

Here  $A$  is the cross sectional area of the basket;  $L$  is the thickness across the modeled section;  $q$  is the uniform heat flux applied over one of the cross sectional area, axial ends; and  $T_i$  is the uniform temperature applied over the other cross sectional area, axial end.  $T_q$  is the average temperature where uniform heat flux is applied and is calculated using the simulation results.

A second option is to apply constant (but different) temperatures at both axial ends of the basket, then calculate the total heat flow ( $qA$ ) through the basket using the simulation results, and lastly calculate the effective axial conductivity using the above equation. To obtain temperature

dependent thermal conductivities, this third step is repeated a number of times using a wide range of uniform circumferential temperatures and applied heat fluxes.

*Fourth*, the thermal conductivities obtained in the third step are added using an equivalent thermal resistor network model to obtain in-plane and axial thermal conductivities, respectively, over the entire fuel basket.

Table IV-14 shows the thermal properties used for the basket. These properties are applied to the homogenized fuel-basket cylinder. The equivalent specific heat and density are obtained using a mass and volume weighted average, respectively, over the individual component properties. The volume of each component in the fuel basket (i.e., support disks, heat transfer disks, fuel tubes, etc.) is given in the Rail-Lead cask SAR.

**Table IV-14. Effective thermal properties of the directly loaded fuel basket**

Effective Thermal Properties	92°C (200°F)	226°C (450°F)	377°C (700°F)	477°C (900°F)	726°C (1340°F)
Radial Thermal Conductivity	3.2 (1.8)	3.8 (2.1)	4.3 (2.4)	5.0 (2.8)	5.9 (3.4)
Axial Thermal Conductivity	2.4 (1.4)	3.2 (1.8)	3.8 (2.1)	4.5 (2.6)	5.8 (3.3)
Specific Heat	332 (0.079)				
Density	2450 (153)				

#### **IV.4.3.2 Neutron Shield Region**

The neutron shield region is modeled using the same approach used in the SARs (NAC International, 2004, Holtec International, 2004). Both reports used the thermal resistor network method to obtain the in-plane and axial effective thermal conductivities (see Section IV.3.3.4). In the case of the Rail-Lead cask, there are fewer radial channels than in the Rail-Steel cask; however, as will be demonstrated shortly, this shortcoming is compensated for by adding copper in the neutron shield region. Table IV-15 shows the thermal properties used for the neutron shield region in the Rail-Lead cask. The circumferential thermal conductivity is assumed to be that of NS-4-FR. As before, the specific heat and density are obtained from a mass and area weighted average. Note the thermal conductivity is slightly higher than in the Rail-Steel cask even though the Rail-Lead cask contains fewer channels. This is expected since the neutron shield in the Rail-Lead cask contains copper which has a much higher thermal conductivity than carbon steel.

**Table IV-15. Effective thermal conductivities for the neutron shield region of the Rail-Lead cask**

Effective Thermal Properties	92°C (200°F)	226°C (450°F)	377°C (700°F)	477°C (900°F)	726°C (1340°F)
In-Plane Thermal Conductivity W/m-°C (Btu/ft-hr-°F)	8.1 (4.6)	7.9 (4.5)	7.7 (4.4)	7.7 (4.4)	7.4 (4.2)
Axial Thermal Conductivity W/m-°C (Btu/ft-hr-°F)	7.6 (4.3)	7.3 (4.2)	7.3 (4.2)	7.2 (4.1)	6.9 (3.9)
Specific Heat J/kg-°C (Btu/lbm-°F)	1406 (0.33)	535 (0.12)	563 (0.13)	575 (0.13)	611 (0.14)
Density kg/m <sup>3</sup> (lbm/ft <sup>3</sup> )	1983 (123)	380 (23)			

#### IV.4.4 Rail-Lead Cask Finite Element Model

The following description is short since most of the details are similar to the Rail-Steel cask analysis described in Section IV.3.4. In the Rail-Lead cask runs, the cask model had 109,662 elements (see Figure IV-19); this corresponds to a nominal element size of 10.2 cm (4 in). The element count is less than in the Rail-Steel cask since the Rail-Lead cask is smaller and has fewer features which add to the element count. A mesh refinement study was also conducted with the Rail-Lead cask model with a similar outcome. The boundary conditions for the normal condition, steady-state run, the regulatory uniform heating run, and the CAFE fire runs are the same as discussed in Sections IV.2 and IV.3.4. They are not repeated here.

Deleted: is

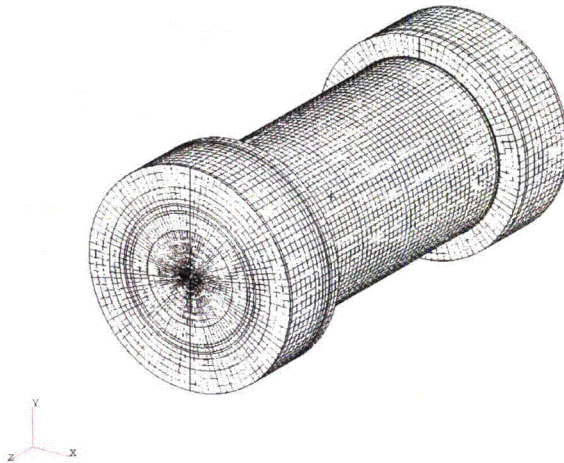


**Figure IV-19. The Rail-Lead cask mesh.**

Overall, maximum temperatures obtained using the model developed here and in the Rail-Lead cask SAR are also similar. Again, the difference in purpose of the two analyses leads to some different assumptions, which in turn leads to slightly different results.

#### **IV.4.5. Rail-Lead Cask Thermal Analysis Results**

The following figures (Figure IV-20 through Figure IV-24) show additional results for the Rail-Lead cask not provided in Chapter 4. Figure IV-20 shows results for the regulatory uniform heating case. Recall this is a P-Thermal only run. Figure IV-21 shows results for the regulatory CAFE fire; Figure IV-22 shows results for the fully engulfing CAFE fire run with the cask on the ground; and Figure IV-23 and Figure IV-24 show results for the CAFE fire runs with the cask on the ground and outside the pool area. As with the Rail-Steel cask, the last three cases are run for a total of three hours. A discussion of these results and their implications is provided in Chapter 4.

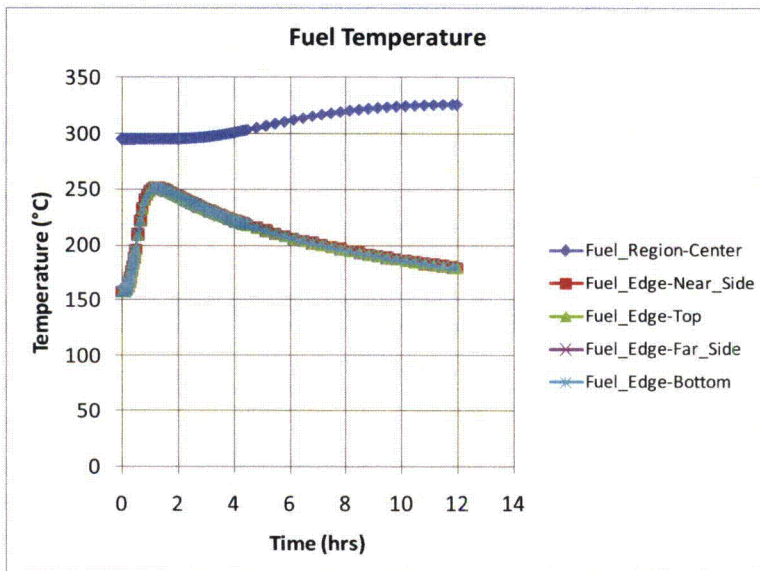
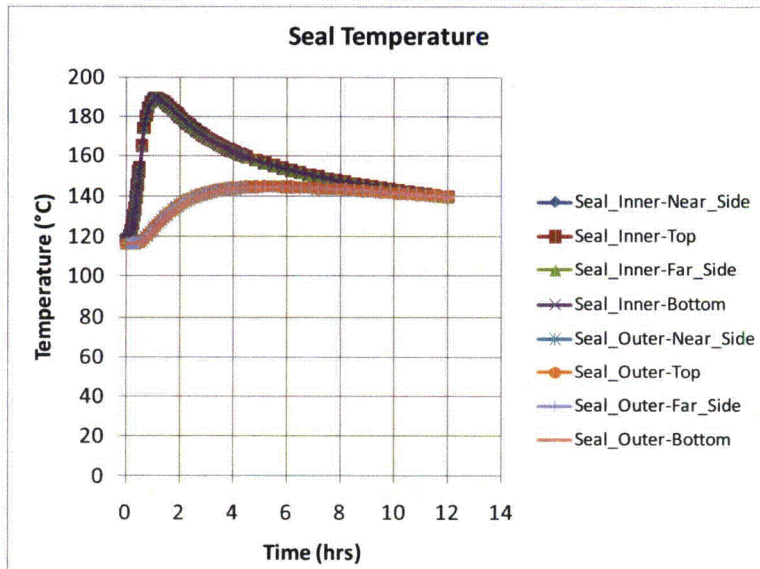


Figure IV-20. Rail-Lead cask regulatory uniform heating results.

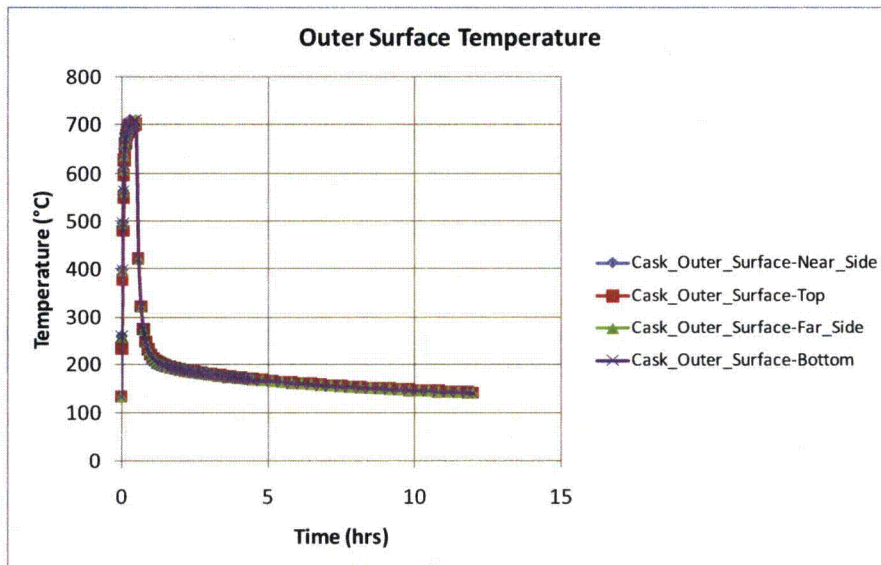
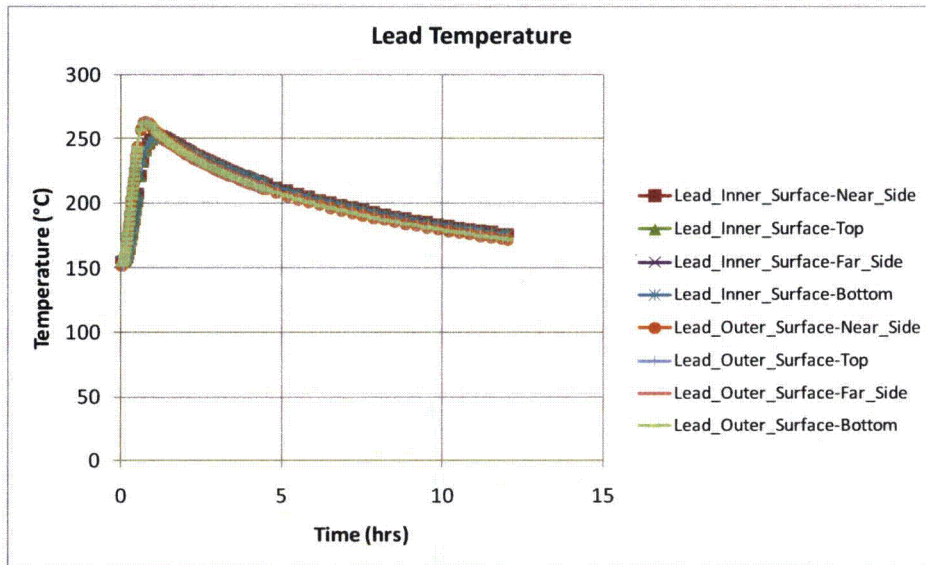


Figure IV-20. Rail-Lead cask regulatory uniform heating results – continued.

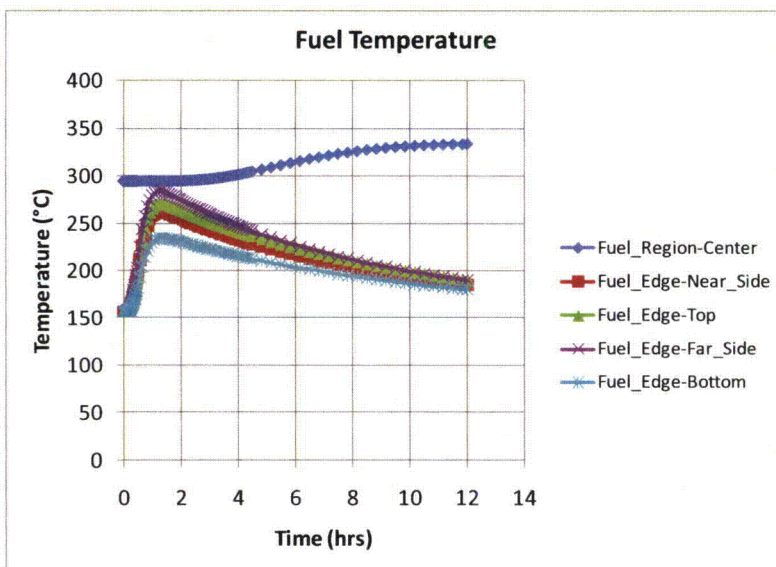
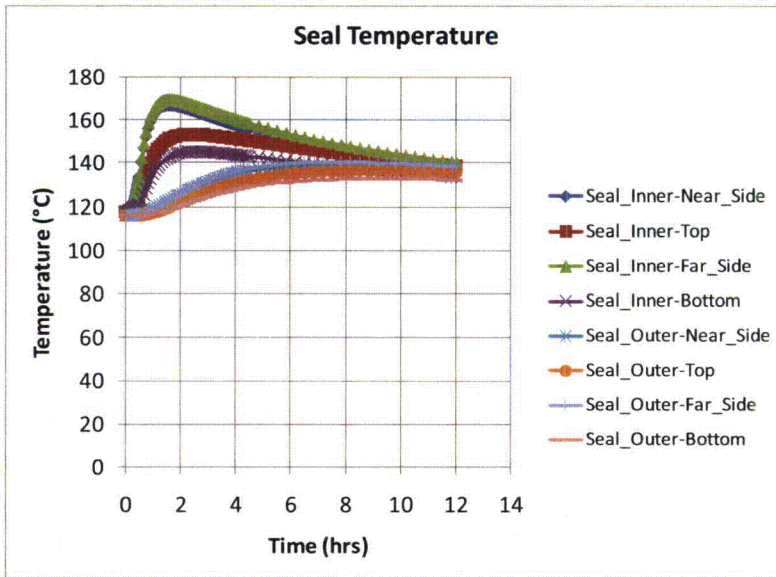


Figure IV-21. Rail-Lead cask CAFE regulatory fire.

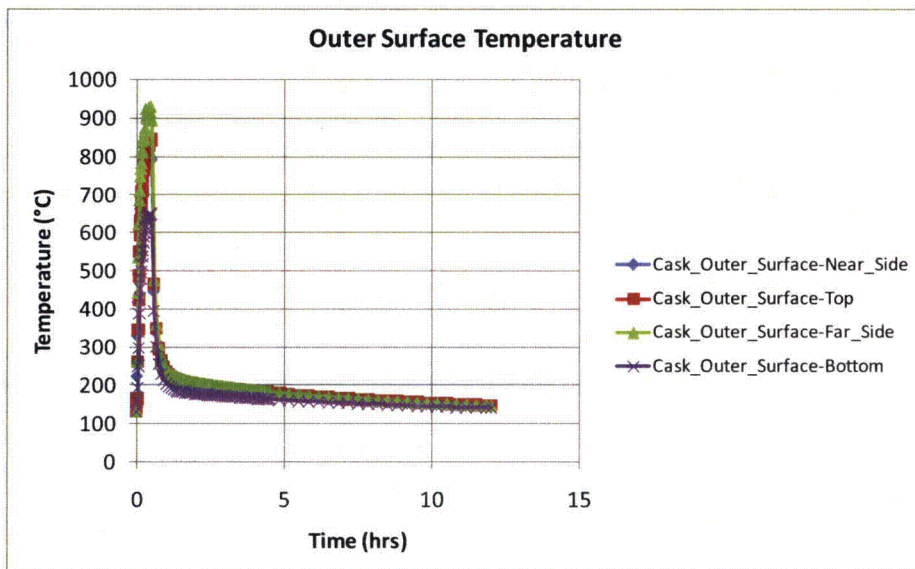
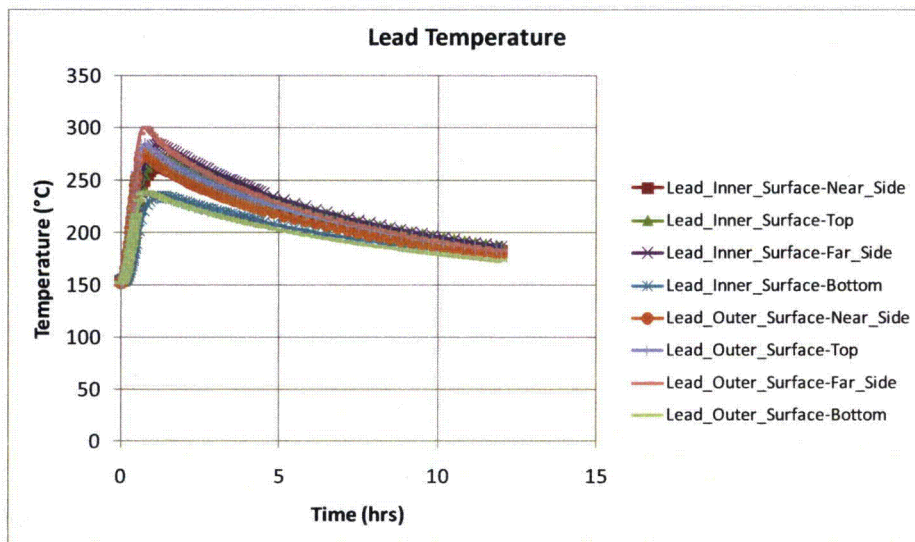


Figure IV-21. Rail-Lead cask CAFE regulatory fire – continued.

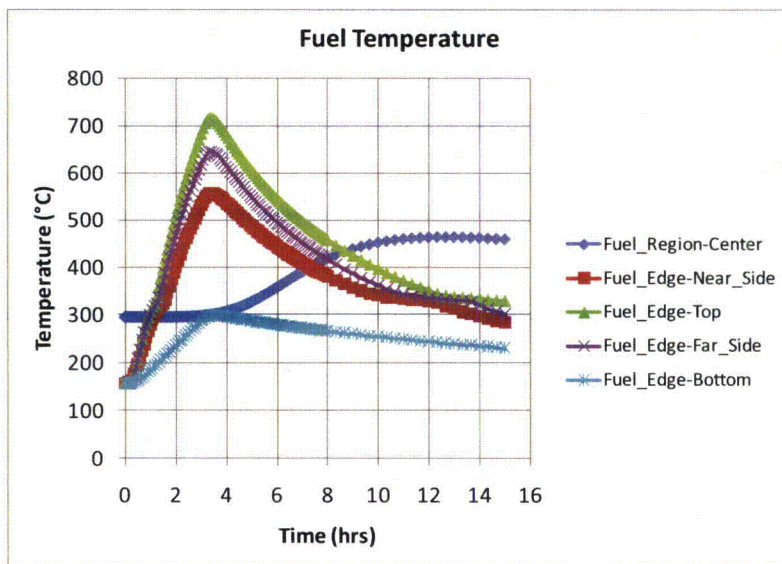
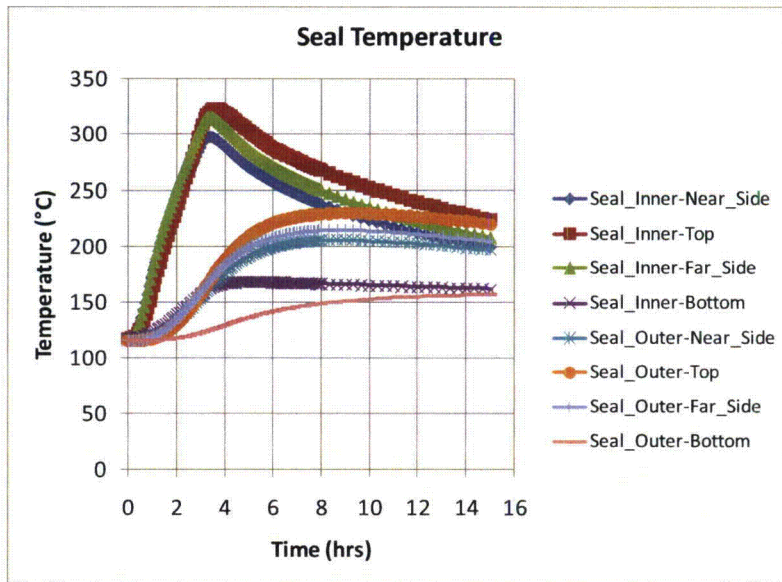


Figure IV-22. Rail-Lead cask on ground at the pool center.

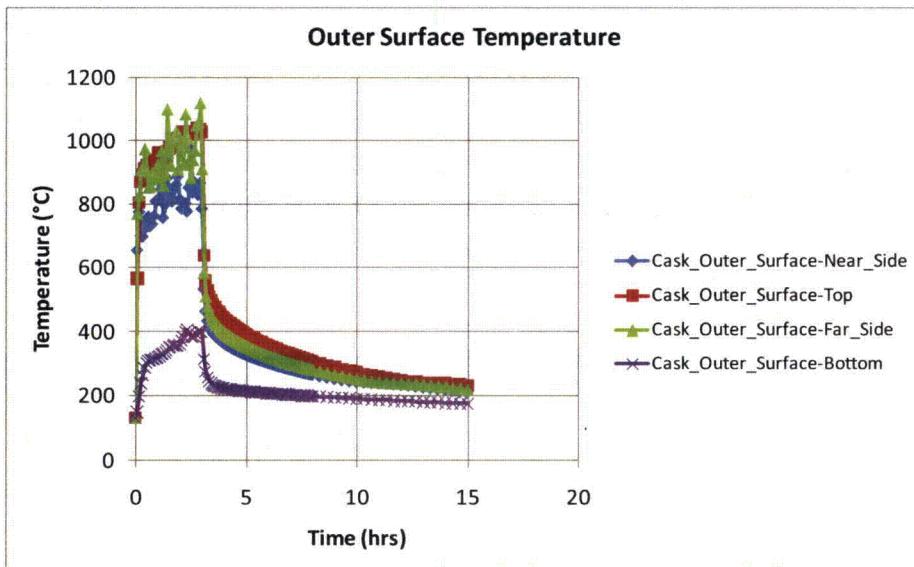
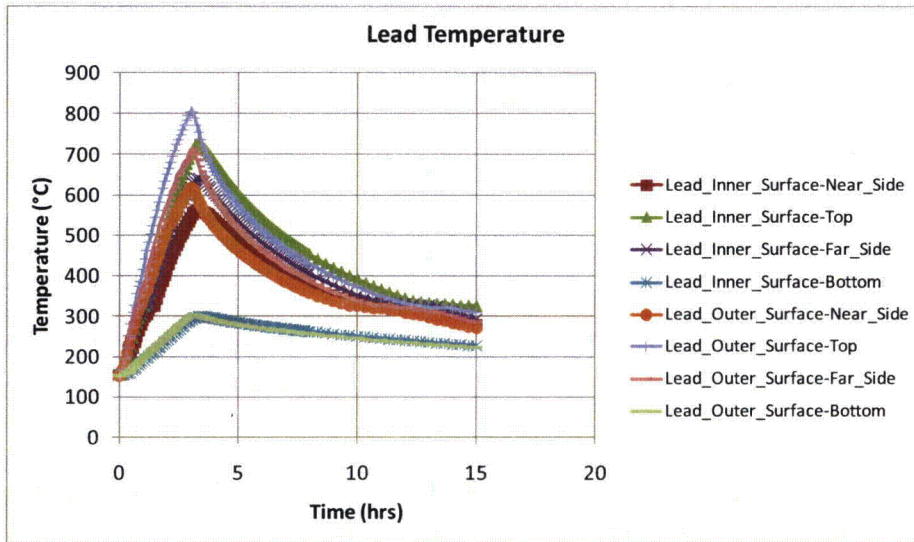


Figure IV-22. Rail-Lead cask on ground at the pool center – continued.

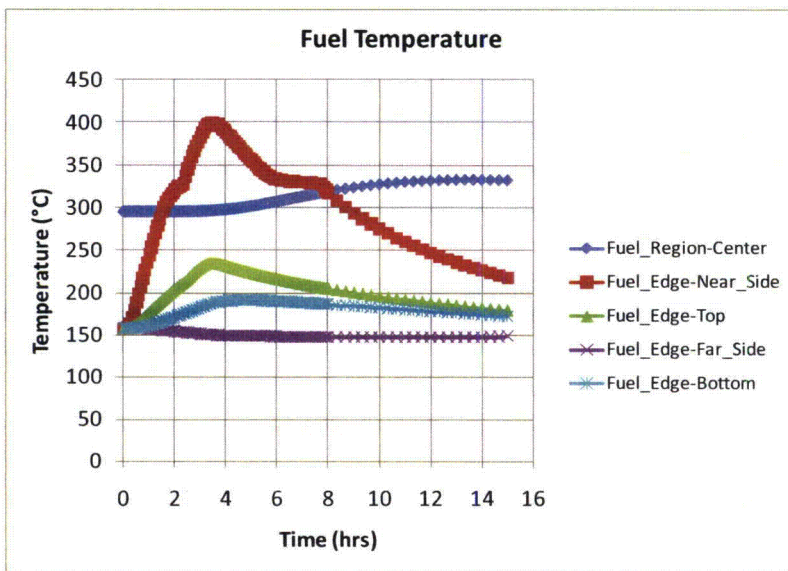
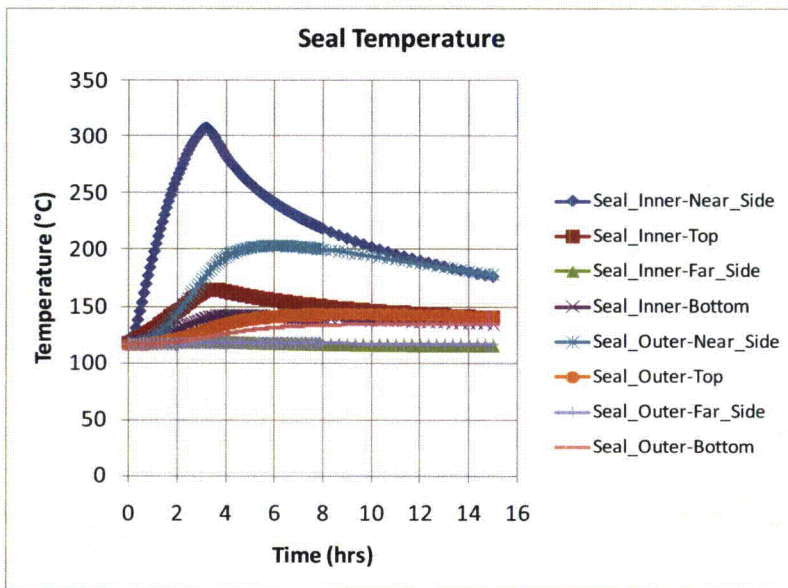


Figure IV-23. Rail-Lead cask on ground 3.0 m (10 ft) from the edge of the pool.

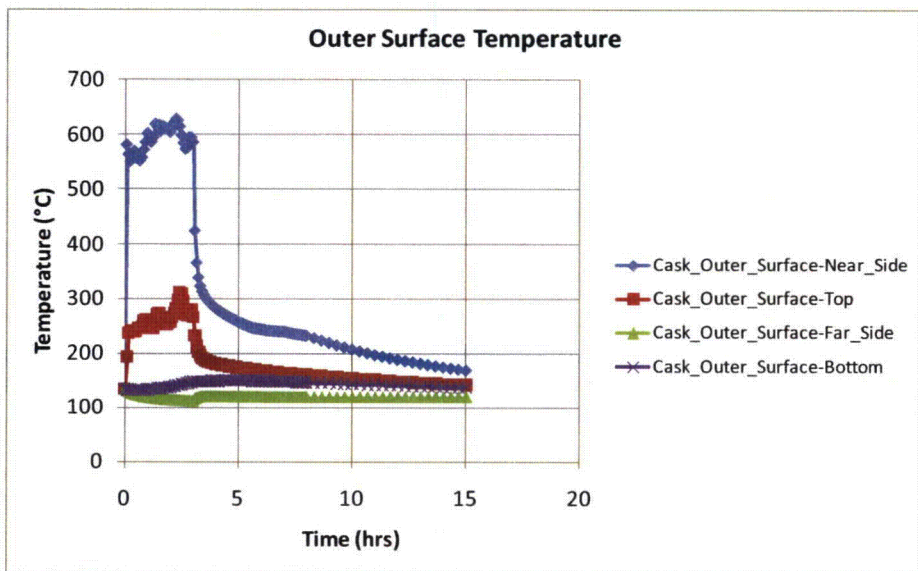
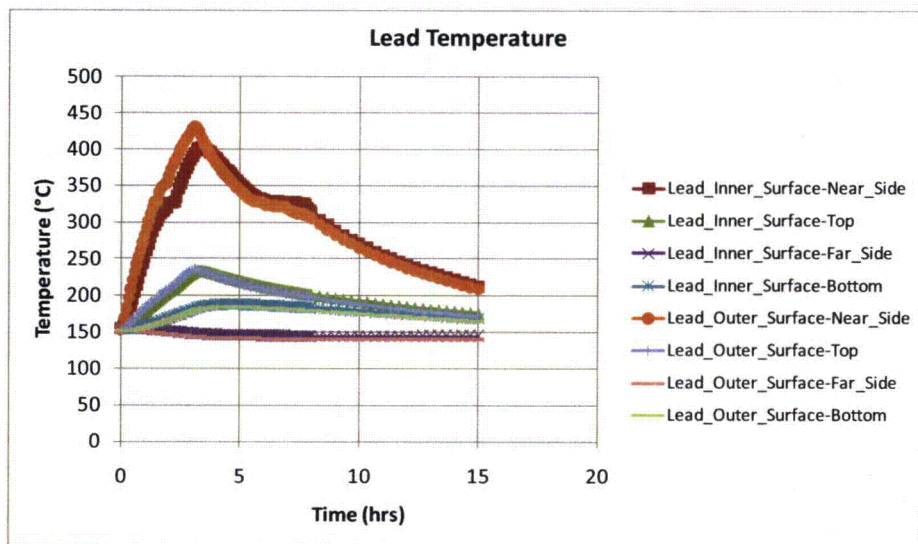


Figure IV-23. Rail-Lead cask on ground 3.0 m (10 ft) from the edge of the pool - continued

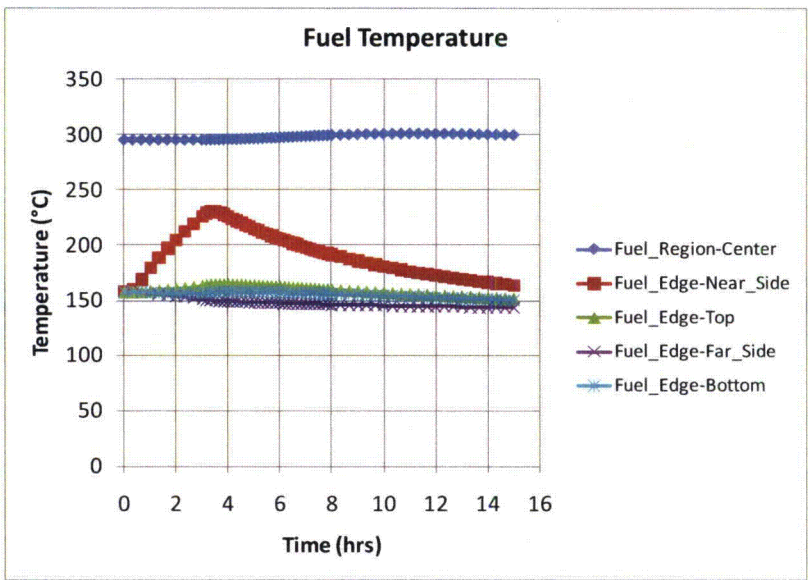
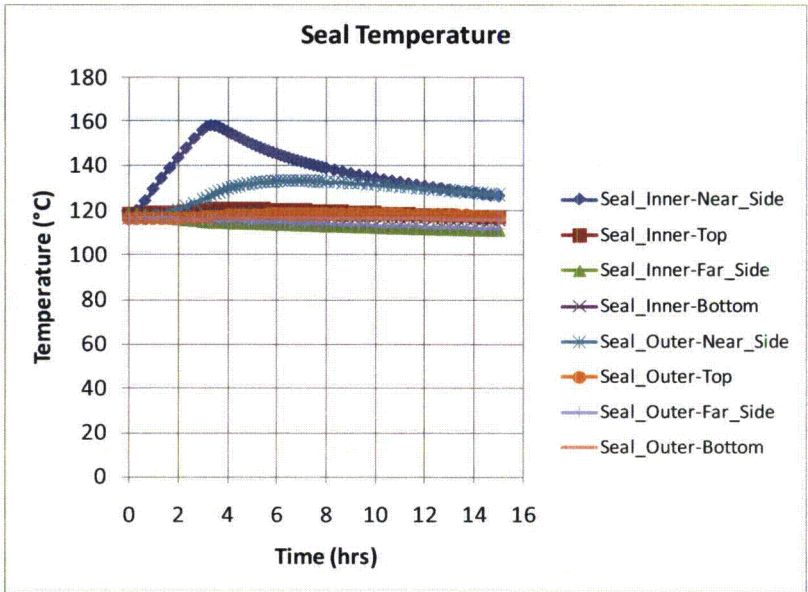


Figure IV-24. Rail-Lead cask on ground 18.3 m (60 ft) from the edge of the pool.

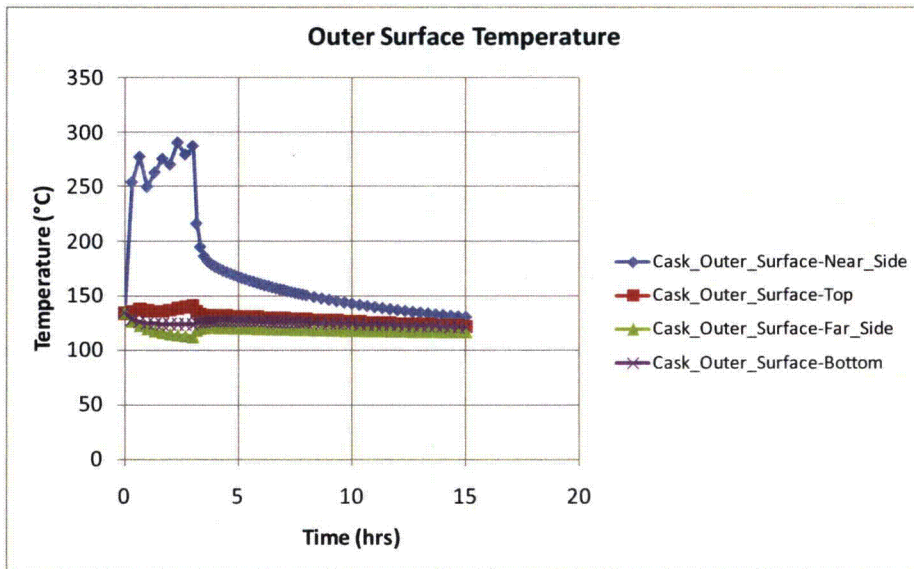
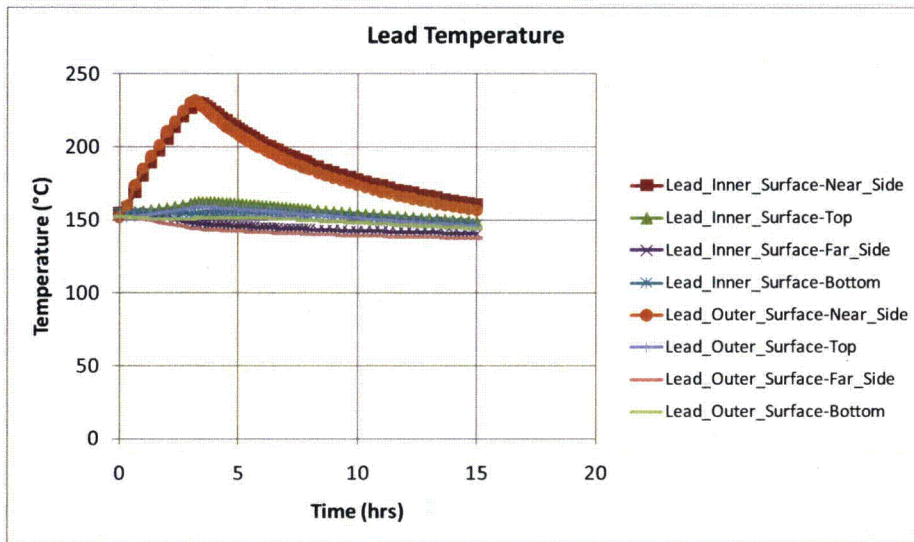


Figure IV-24. Rail-Lead cask on ground 18.3 m (60 ft) from the edge of the pool – continued.

## IV.5 Truck Cask with Depleted Uranium

The Truck-DU cask is slightly different from the two previously analyzed casks. This cask is certified to transport up to four PWR spent fuel assemblies on a truck flat bed and uses depleted uranium for the gamma shield. In this analysis, the cask is assumed to be in the horizontal configuration, as it would most likely be after an accident scenario. For the Truck-DU cask, results reported in the Truck-DU FDR (General Atomics, 1993) are used, but modified where necessary to reflect the current study.

### IV.5.1 Geometric Considerations

The Truck-DU consists of an overpack, a fuel basket, and limiters at each end. Like the Rail-Lead cask, the Truck-DU is a single containment cask with no MPC. Compared to the Rail-Steel and Rail-Lead casks, however, this cask is smaller in size [1.00 m (39.8 in) in diameter at the center, 2.3 m (90 in) in diameter at the impact limiters, and 5.94 m (234 in) in length] since it carries only four spent fuel assemblies. Figure IV-25 shows the layout of the Truck-DU cask.

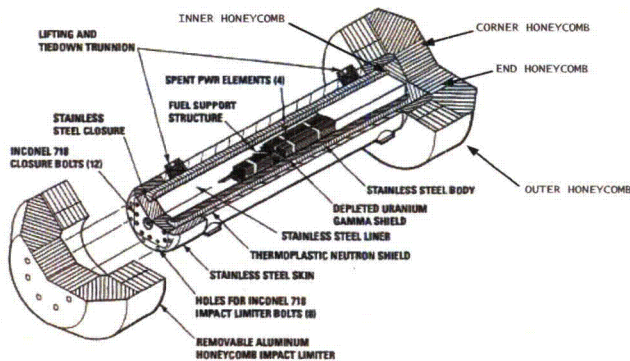


Figure IV-25. Components of Truck-DU cask (General Atomics 1993).

#### IV.5.1.1 Fuel Assembly and Interior Cavity of the Overpack

The inner cavity of the Truck-DU is a rectangular box 0.46×0.46 m (18×18 in) in the cross section and 4.25 m (167 in) long. Inside this cavity, the fuel assemblies are stored within four slots formed by a steel fuel-support structure (FSS). The details of the fuel assembly are discussed in Section IV.3.1.2. The FSS is made from four panels [0.016 m (0.61 in) thick] arranged in a perpendicular cross pattern. The fuel assembly and FSS together are referred to as the fuel basket in this section. Fuel spacers and other support structures complete the remaining space at the ends of the fuel basket. These regions are referred to in this section as the fuel basket ends.

In this analysis, the fuel basket and the fuel basket end regions are each represented as single volumes to minimize geometric complexity, but their thermal response is accounted for using effective properties.

#### **IV.5.1.2 Overpack**

The overpack center cross section is made from a five-layer cross section. The first three inner layers are square with rounded corners. The first layer, the cavity liner, is a thin steel wall [9.5 mm (0.376 in) thick] that separates the contents of the cask from the gamma shield. The second layer is a thick wall [6.7 cm (2.6 in) at the center of the cask] of depleted uranium which serves as the gamma shield. The third, and last square layer, is a thick wall [7.6 cm (3 in)] of steel. In the axial direction, the depleted uranium layer tapers off and extends just past the ends of the inner cavity of the overpack. The cavity liner and the thick steel wall extend almost to the axial ends of the gamma shield. The cavity liner and the thick steel wall mate with a square shaped, steel flange at the top of the overpack and a square shaped, metal base cup at the bottom. The inner cavity of the overpack is sealed off from the environment using a steel lid [0.28 m (11 in) thick at the center] which fits on the flange as shown in Figure IV-25. The metal base cup is 0.24 m (9.5 in) thick.

The last two layers, the neutron shield and the thin steel outer skin wall [1 cm (0.4 in) thick], form the rest of the center cross section of the overpack. The outer surface of the neutron shield layer and the outer skin wall are circular in shape. In the axial direction, the neutron shield and the outer skin wall extend the interior plane wall of the impact limiters. Both layers mate with an Impact Limiter Support Structure (ILSS) at these extreme ends. The ILSS is design to support the impact limiters using a series of ribs, 1.9 cm (0.75 in) thick, that extend radially outward from the exterior surface of the thick steel wall to the interior surface of the outer shell wall of the ILSS. The space between these ribs and between the exterior surface of the thick steel wall and the interior surface of the outer shell wall of the ILSS is filled with a neutron shield material. In the axial direction, the ILSS extends to the end of the lid at the top, and to the metal base cup at the bottom.

Deleted: of the

The cavity liner, gamma shield, thick steel wall, flange, base metal cup, lid, neutron shield region, and outer skin wall are represented explicitly in the thermal model with minor alterations to simplify the model. The ILSS are represented as single volumes to minimize geometric complexity, but their thermal response is accounted for appropriately using effective properties. As with the Rail casks, the Truck-DU cask overpack contains a number of features that serve a special purpose (e.g., valves, seals, trunnions, etc.) These features are omitted from the model as is done in the previous rail cask models and for the same reasons: (1) negligible due to their small volume and mass relative to the other components in the overpack, (2) highly localized with no effect to the overall thermal performance of the cask at locations of interest, or (3) both.

#### **IV.5.1.3 Impact Limiters**

The Truck-DU cask, impact limiters bolt to the top and bottom of the overpack. These impact limiters are similar to the Rail-Steel limiters in that they are made of aluminum honeycomb material encased in a thin steel shell. The honeycomb material is arranged as shown in Figure IV-25.

In this model, the impact limiters were assumed undamaged; hence, they are modeled using the geometry shown in Figure IV-25. The encasing steel shell is neglected since the total volume of the shell is small compared to the rest of the honeycomb material.

#### IV.5.2. Truck-DU Thermal Behavior and Model Assumptions

Like the Rail casks, the Truck-DU cask is designed to release heat passively under normal conditions of transport. The Truck-DU fuel basket is designed to accommodate a maximum heat load of 2468 W (a maximum of four fuel assemblies at 617 W per assembly). Table IV-16 shows the normalized, axial heat generation rate distribution for a 617 W PWR assembly. This axial heat generation profile is applied over the active fuel region which encompasses only about 3.66 m (144 in) of the total fuel assembly length.

Table IV-16. Axial burn up profile in the active fuel region of the Truck-DU cask

Axial Distance from Bottom of Active Fuel (% of Active Fuel Length)	Normalized Value
0-1.4	0.432
1.4-4.2	0.630
4.2-7.6	0.847
7.6-11.1	0.964
11.1-15.3	1.09
15.3-24.3	1.22
24.3-38.9	1.22
38.9-66.0	1.09
66.0-77.9	0.964
77.9-84.7	0.847
84.7-91.7	0.630
91.7-96.3	0.432
96.3-100	0.252

As with the Rail casks, heat is dissipated from the fuel rods to the exterior surfaces of the Truck-DU cask by a combination of conduction, convection, and radiation heat transfer. Heat transfer from the fuel assemblies to the outer surface of the overpack and the limiters is similar to the other rail casks. The only exception is there are fewer large voids through the cross section of this cask. Heat dissipation from the center cross section of the cask is predominately by conduction and radiation through the fuel assembly and the FSS. Conduction dominates through the overpack cross-section. In the axial direction, radiation occurs between the ends of the fuel assembly and inner cavity wall. Conduction through the honeycomb material is complex; however, effective properties found in the Truck-DU cask FDR are used to obtain the thermal response of the impact limiters.

The Truck-DU cask is also designed to maintain the temperature of critical components below their design limits during and after a 30 minute, fully engulfing, hypothetical accident condition (HAC) scenario. For fire accident scenarios lasting longer than the HAC fire described in 10 CFR 71.73, a significant amount of heat may be transferred to the interior of the cask. As in the rail casks, the temperature of the neutron shield material is expected to reach temperatures beyond its operational temperature limit. Heat then is assumed to be dissipated by conduction through a gas layer in the neutron shield region and by radiation between the outer surface of the thick steel wall layer and the inner surface of the outer skin wall.

### **IV.5.3 Truck-DU Materials and Thermal Properties**

The Truck-DU cask is made of stainless steel, depleted uranium, copper, aluminum, polypropylene, Boral neutron absorber ( $B_4C$ ), and helium. With the exception of spacers, bolts, and the lifting trunnions, which are all ignored in this analysis, all major components of the overpack are made from stainless steel, type XM-19. The outer skin wall of the overpack is made from a combination of XM-19 and copper. The stainless steel serves as the main support component while the copper enhances conduction in the axial direction. The neutron shield material is made from polypropylene which has a melting point above  $149^{\circ}C$  ( $300^{\circ}F$ ). The impact limiters are made from various density aluminum alloy materials. The stainless steel shell (XM-11 and XM-19) encasing the honeycomb material is ignored in this study. As with previous fuel basket wall materials, the FSS is made from stainless steel and  $B_4C$ .

With the exception of XM-19 and the honeycomb material, all material properties can be found in Sections IV.3.3 and IV.4.3. Table IV-17 and Table IV-18 show the material properties used for XM-19 and the honeycomb material. The honeycomb material is classified by location in the limiter (see Figure IV-25).

#### ***IV.5.3.1 Effective Thermal Properties***

Effective properties were used for the active fuel basket region, the ends of the fuel basket, the neutron shield region, the ILSS region, and the outer skin wall (see Table IV-19 and Table IV-20). These properties were obtained from the Truck-DU cask FDR (General Atomics, 1993). For the HAC scenarios, the polypropylene material was replaced with air above  $149^{\circ}C$  ( $300^{\circ}F$ ) since polypropylene melts at relatively low temperatures. Recall that radiation heat transfer was added between the outer surface of the thick steel wall layer and the inner surface of the outer skin wall to increase heat transfer to the interior of the cask during the fire as was done in previous rail cask analysis.

**Table IV-17. Thermal conductivities for the Truck-DU cask materials**

Material	Thermal Conductivity W/m-°C (Btu/hr-ft-°F)				
	92°C (200°F)	226°C (450°F)	377°C (700°F)	477°C (900°F)	726°C (1340°F)
XM-19	12.3 (7.1)	15.2 (8.8)	17.0 (9.8)	18.7 (10.7)	22.8 (13.2)
Inner Honeycomb $k_r/k_z$	8.7/2.6 (5.0/1.5)				
Outer Honeycomb $k_r/k_z$	6.5/2.0 (3.8/1.2)				
Corner Honeycomb $k_r/k_z$	1.7/2.9 (0.98/1.8)				
End Honeycomb $k_r/k_z$	2.6/8.6 (1.5/5.0)				

**Table IV-18. Volumetric Specific heat for the Truck-DU cask materials**

Material	Volumetric Specific Heat ( $\rho C_p$ ) J/m <sup>3</sup> -°C (Btu/ft <sup>3</sup> -°F)
XM-19	4287264 (37242)
Inner Honeycomb	1553000 (41.7)
Outer Honeycomb	117000 (3.1)
Corner Honeycomb	39290 (1.05)
End Honeycomb	1553000 (41.7)

**Table IV-19. Effective thermal conductivities for the Truck-DU cask materials**

Material	Thermal Conductivity W/m-°C (Btu/hr-ft-°F)				
	92°C (200°F)	226°C (450°F)	377°C (700°F)	477°C (900°F)	726°C (1340°F)
Active Fuel Region $k_r/k_z$	1.2/4.5 (1.0/3.8)	1.8/4.9 (1.5/4.2)	2.3/5.2 (2.0/4.4)	2.8/5.7 (2.4/4.9)	4.9/7.3 (4.2/6.2)
Fuel Region Ends $k_r/k_z$	0.28/3.3 (0.24/2.8)	0.31/3.8 (0.26/3.2)	0.33/4.1 (0.28/3.5)	0.35/4.6 (0.30/3.9)	0.40/6.3 (0.34/5.3)
Neutron Shield Region $k_r/k_z$	1.7/0.15 (1.5/0.12)				
ILSS $k_{r\_bottom}/k_{r\_top}/k_z$	2.2/3.9/0.85 (1.8/3.3/0.72)	2.8/4.9/1.0 (2.3/4.1/0.85)	3.2/5.6/1.2 (2.7/4.8/1.0)	3.5/6.1/1.3 (3.0/5.2/1.1)	4.2/7.5/1.5 (3.6/6.4/1.3)
Outer Skin Wall $k_r/k_z$	12.2/41.5 (10.4/35.4)	15.2/44.0 (13.0/37.5)	17.0/45.5 (14.5/38.8)	18.6/47.0 (15.9/40.0)	22.8/50.3 (19.4/42.9)

**Table IV-20. Effective volumetric specific heat for the Truck-DU cask materials**

Material	Volumetric Specific Heat ( $\rho C_p$ ) J/m <sup>3</sup> -°C (Btu/ft <sup>3</sup> -°F)
Active Fuel Region	938700 (25.2)
Fuel Region Ends	1263000 (33.9)
Neutron Region	1715000 (46.0)
ILSS	1225000 (32.8)
Outer Skin Wall	3882000 (104.2)

#### IV.5.4 Truck-DU P-Thermal Finite Element Model

In the Truck-DU runs, the cask model had 241,700 elements (see Figure IV-26). The element count is higher than in the rail cask analysis since the Truck-DU has a number of smaller features that add to the element count. The boundary conditions for the normal condition, steady-state run; the regulatory uniform heating run; and the CAFE fire run are the same as discussed in Sections IV.2 and IV.3.4. In this analysis, the fire is run for only one hour. This time frame corresponds to the total fuel burning time for the maximum capacity, fully loaded, fuel tanker truck.

Overall, maximum temperatures obtained in the normal condition, steady state run and in the regulatory uniform heating case using the model developed here are similar the results presented in the Truck-DU cask FDR. Again, the difference in purpose of the two analyses leads to some different assumptions, which in turn leads to slightly different results.

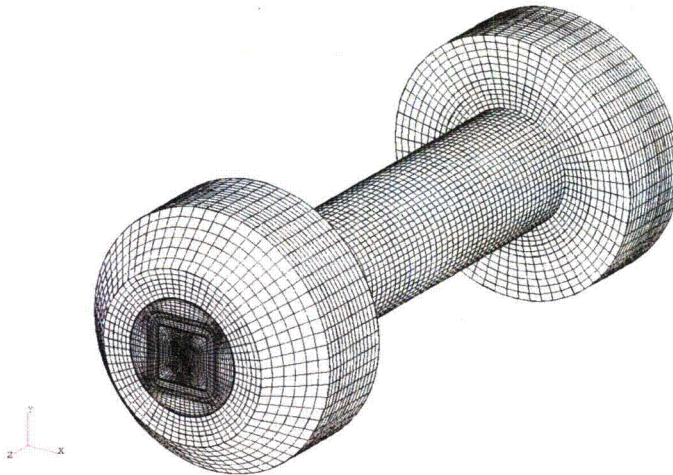


Figure IV-26. Truck-DU cask mesh.

#### IV.5.5 Truck-DU Cask Thermal Analysis Results

Recall that for the Truck-DU cask, only one CAFE non-regulatory fire is run: the cask on ground and at the center of the pool (see Figure IV-27). This is the most severe case as demonstrated in the Rail-Steel and Rail-Lead cask analysis. Figure IV-28 shows additional results for this case not provided in Chapter 4. A discussion of these results and their implications is provided in Chapter 4.

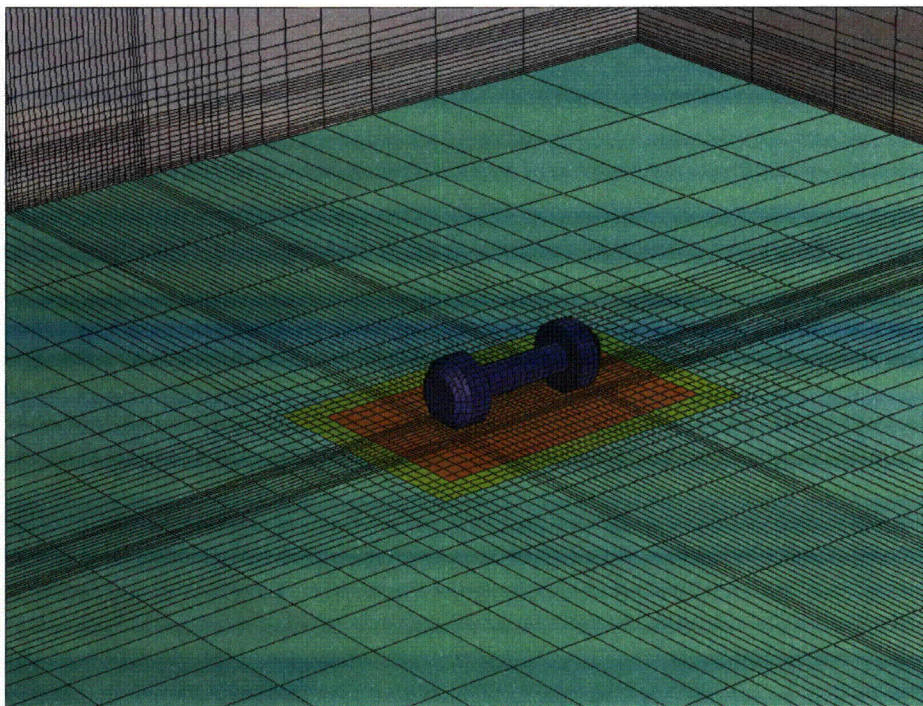


Figure IV-27. CAFE three-dimensional domain with Truck-DU cask on ground.

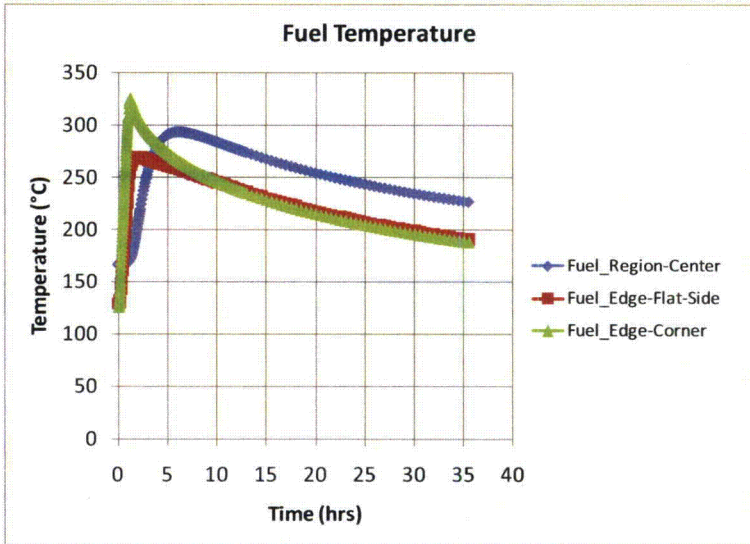
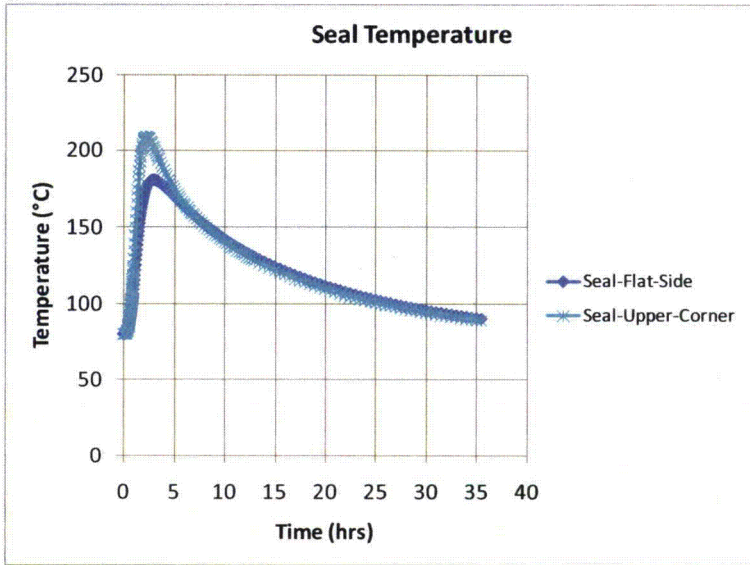


Figure IV-28. Truck-DU cask on ground at the pool center.

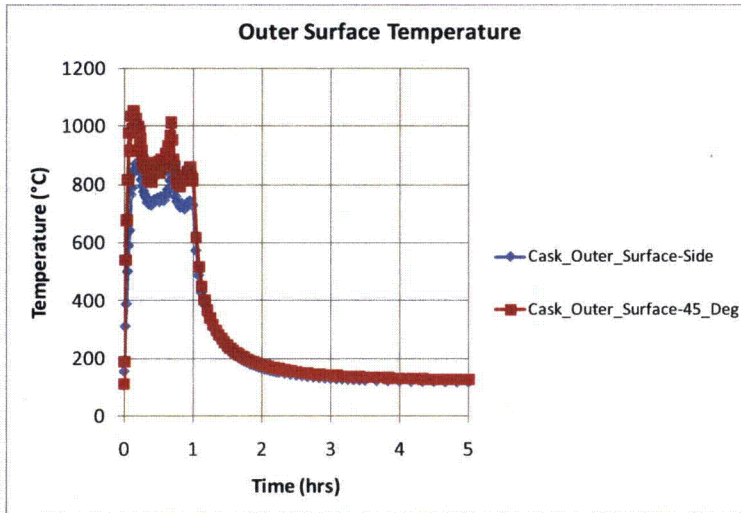


Figure IV-28. Truck-DU cask on ground at the pool center – continued.

#### IV.6 CAFE Benchmark

Large, fully-engulfed objects have a great impact on the surrounding fire environment. To adequately predict incident heat flux to casks, computational fluid dynamics models must be employed with appropriate boundary conditions. Also, because of the impact that massive objects have on fires, computational fluid dynamics models must be validated against experimental data from tests that have similar size objects (Nicolette and Larson, 1989).

Since the development of the CAFE code (del Valle, et. al., 2009; del Valle, 2007; Are, et.al., 2005; Lopez, et. al., 2003), there has been a continuing effort to benchmark and fine-tune this fire model by making use of relevant empirical data from experiments. Continuing with this effort, prior to running the cases described in Chapter 4, CAFE is benchmarked against experimental data obtained from two fire test series conducted at Sandia National Laboratory Lurance Canyon Burn Site: (1) one using a large calorimeter in the center of the pool (Greiner, 2009; Kramer, 2008), and (2) the other using a smaller diameter calorimeter adjacent to the fire (Lopez et. al., 2003). The large calorimeter is close to the size of the casks analyzed in this study, and had a test setup and conditions that closely matched the regulatory hypothetical fire accident scenario outlined in 10 CFR 71.73 for certification of SNF transportation casks. The smaller diameter calorimeter test is used to benchmark CAFE's ability to predict heat flux to objects outside the fire plume. This section briefly describes these experiments, and shows benchmark results.

#### IV.6.1 Large Calorimeter Test and Benchmark Results

The large calorimeter is a carbon steel cylindrical pipe approximately 2.43 m (96 in) in diameter and 4.6 m (180 in) in length, with nominal 2.54 cm (1 in) thick walls, and had bolted lids on each end [see Figure IV-29(a)]. The calorimeter is placed on two stands at the center of a 7.93m (26ft) diameter fuel pool. The stands maintained the calorimeter 1m (39.4in) above the fuel surface. Approximately 2000 gallons of JP8 are used per test. Total burn time vary with tests, but is at least 25 minutes. All tests are conducted in relatively low wind conditions (<5m/s) to assure the calorimeter is fully or partially engulfed [see Figure IV-29(b)].

Thermocouples are installed on the interior walls of the calorimeter to measure interior surface temperatures. All TCs are installed in a ring configuration as shown in Figure IV-30. Heat flux gages are placed just outside the round walls of the calorimeter in a ring configuration and outside the lids to measure incident heat fluxes close to the outer walls of the calorimeter. Fuel burn rates are measured using a TC rake—a linear array of TCs traversing the depth of the fuel layer at known distance intervals. Directional flow probes are installed just outside of the calorimeter walls to measure the flow speed of hot gases near the calorimeter walls. Finally, ultrasonic sensors placed on four towers—two sensor towers aligned with the calorimeter lids and two sensor towers perpendicular to the cylindrical section of the calorimeter, but on opposite sides—are used to measure wind speed and wind direction. Each tower is approximately 24.4 m (80 ft) from the center of the pool and had three ultrasonic sensors 2, 8 and 10 m (6.5, 26.2, and 32.8 ft) from the ground.

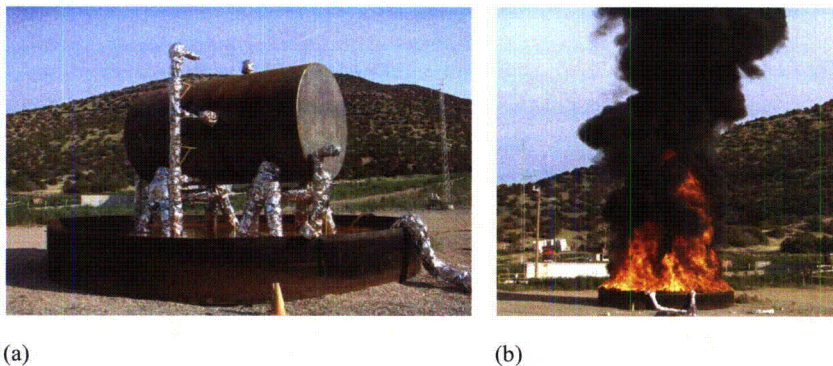


**Figure IV-29. Large calorimeter fire test: (a) test setup and (b) fire fully engulfing the calorimeter.**

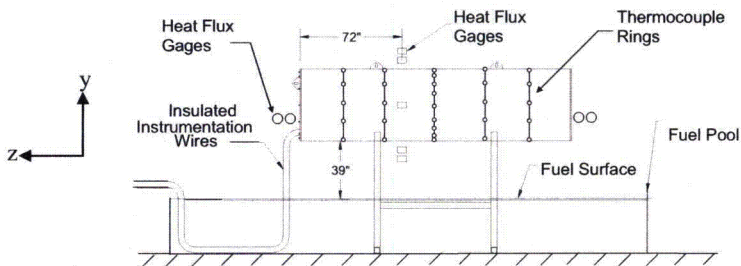
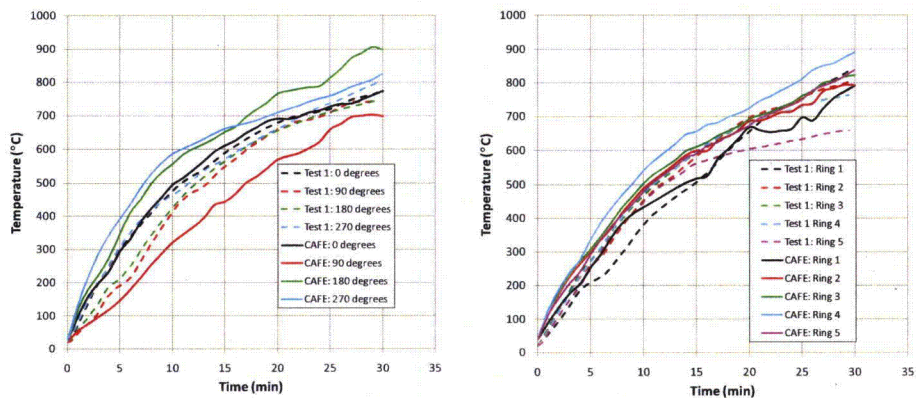


Figure IV-30. Side view (looking from the north) of calorimeter and test setup. Note: the calorimeter is centered with the pool. This drawing is not to scale.

Figure IV-31a shows average temperatures along the four circumferential sides of the calorimeter obtained from Test 1 and from the CAFE benchmark run. Data from Test 1 is chosen because the wind conditions and fire characteristics of this test best matched the regulatory conditions specified in 10 CFR 71.73 and the fire scenarios analyzed in this study. The test readings are taken from thermocouples located at 0 (north side, i.e., pointing out of the page), 90 (top side), 180 (south side, i.e., pointing into the page) and 270 (underneath) degrees. This plot illustrates that average temperature predictions obtained from CAFE envelope the average temperatures readings from the test.



(a)

(b)

Figure IV-31. CAFE benchmark results using fully engulfed large calorimeter: (a) temperatures average along the 0, 90, 180, and 270 degree side looking at the calorimeter from the negative z-direction, and (b) temperatures averaged over each ring starting from Ring 1 located on the positive side of the z-axis.

From this perspective, CAFE over predicts temperatures underneath and on the south side of the calorimeter, and under predicts temperatures on the top of the calorimeter. Figure IV-31b shows a plot of average temperatures over each thermocouple ring starting from the left side of the calorimeter and moving along the negative z-axis as shown in Figure IV-30. From this perspective CAFE predicts the average temperatures over the rings reasonably well.

Closer inspection of the temperatures histories obtained from CAFE at each of the nodes corresponding to thermocouple locations revealed excellent agreement with test data over most of the cask, except at locations where the wind effects are strongest, the last two rings to the right of Figure IV-30 at 90 (top side), 180 (south side) and 270 (underneath) degrees. Temperatures at 180 and 270 degrees are higher than expected, while temperatures at 90 degrees are under predicted. Differences rapidly diminished going from the rings on the right side of the calorimeter to the rings on the left side as shown in Figure IV-30. Part of the reason for these discrepancies is the way in which the wind boundary conditions are applied in the computational fluid dynamics model. In the large calorimeter test series, wind speeds are obtained only at four locations around the pool, and at three heights. These height dependent data are applied uniformly over the corresponding cross sections of the domain, which does not necessarily reflect the actual conditions in the test. This leads to wind speeds being higher than expected in some locations around the casks such as the south side of the cask near the ring 5 (rightmost ring in Figure IV-30).

#### **IV.6.2 Small Calorimeter Test and Benchmark Results**

Experimental data from a smaller pipe calorimeter is used to benchmark the view factor method used in CAFE (Lopez, et al., 2003). The CAFE model for thermal radiation transport within and near large hydrocarbon fires is divided into two types, diffusive radiation inside the flame zone and clear air or view factor radiation outside the flame zone. Outside the flame zone, thermal radiation transport is modeled by the clear air or view factor method. The calculation of the view factor between the fire and an adjacent object is complicated due to the fact that the outer surface of a fire (or smoky region) is dynamically changing due to the puffing and turbulent nature of flames (Lopez, et. al., 2003).

In the experiments, a calorimeter is positioned such that its axis is 1.5 m (4.9 ft) away from the center of the fuel pool. The wind blew the fire away from the calorimeter leaving a significantly larger gap between the pipe calorimeter and the plume. Results from tests and CAFE are presented in Figure IV-32. The temperatures shown are at the center ring of this calorimeter. The blue lines are obtained from experimental data and the black lines are obtained from CAFE. By looking at the temperature distribution of this very long pipe, it can be clearly seen how the external radiation algorithm worked on the far field object.

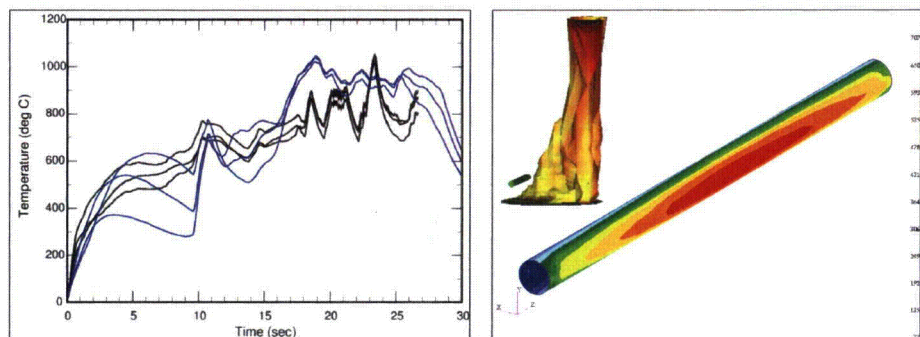


Figure IV-32. CAFE benchmark results using a small calorimeter 1.5m (4.9ft) from the edge of the fire.

#### IV.6.3 Summary of Benchmark Results

The fully engulfing benchmark results show that CAFE bounds the experimental calorimeter temperatures. Inside the fire, CAFE under estimates temperatures near the top of the calorimeter, while it over estimates temperatures on all other sides of the calorimeter. Taken as a whole, these results show that CAFE slightly over predicts the average temperature of the surface of the calorimeter. Therefore, it is expected that for the fully engulfing cases examined in this study, the cask surface temperatures predicted by CAFE will be close to or slightly higher than expected.

Outside the fire zone, CAFE is expected to predict reasonably accurate temperatures for objects near the fire. For objects further from the pool, results are expected to be less accurate given the method employed by the code. This is not a concern since the heat flux to objects outside the plume decreases with the distance squared, suggesting that the fire threat is also less severe with distance from the fuel pool as observed in the results for the 18.3 m (60 ft) standoff case.

#### IV.7 Summary

This appendix described the method employed to obtain the thermal response of the Rail-Steel, Rail-Lead, and Truck-DU casks to several fires lasting longer than the HAC fire described in 10 CFR 71.73.

The approach used to model internals of these casks is similar to that presented in respective cask SARs and in the Truck-DU cask FDR. Some mathematical models and results reported in these documents and used in this study are described in this appendix. In addition, modifications made to the cask models to simplify the complexities inherent in the cask design are noted. In general, boundary conditions and material properties are slightly different from those used in SARs. For consistency, the same properties are used in these casks where the same or similar type materials are used. Since realistic boundary conditions are sometimes difficult to implement using available data and/or current analysis tools, some simplifications also had to be made.

MSC PATRAN is the front end code employed to generate the material database, the finite element discretization, and the boundary conditions for the internals of the casks. P-Thermal is the finite element heat transfer code used to solve the internal thermal response of the casks. CAFE is the computational fluid dynamics (CFD) code used to generate the fire environment for the hypothetical fires lasting longer than the hypothetical fire described in 10 CFR 71.73. For these scenarios, CAFE and P-Thermal are coupled together to obtain the thermal response of the casks. P-Thermal is also used to generate the regulatory fire environments used for model verification. Results from these P-Thermal regulatory fires were compared against results presented in the SARs for the same regulatory environments. This served as a check to the current models.

Four fire accident scenarios are analyzed for the rail casks (and one hypothetical fire accident scenario, the worst case in the rail cask analyses, is analyzed for the truck cask). These are the regulatory fire described in 10 CFR 71.73, a cask on the ground concentric with a fuel pool sufficiently large to engulf the cask, a cask on the ground with a pool fire offset by the width of a rail car (3 meters), and a cask on the ground with a pool fire offset by the length of a rail car (18 meters). These non-regulatory scenarios represent an accident in which a pool of flammable liquid and the cask are separated by one rail car width or one rail car length following an accident. The results shown in this section demonstrate that the Rail-Steel, Rail-Lead, and Truck-DU casks maintain containment for the cases analyzed in this study.

Deleted: -----Page Break -----  
¶  
¶